Impact of Fuel Type on Fire Dynamics in Mechanically Ventilated Compartment as a Consequence of Closing Inlet Vent

Brady Manescau, Hui-Ying Wang, Jean Pierre Garo, Bruno Coudour, Lahna Acherar

Impact of fuel type on fire dynamics in mechanically ventilated compartment as a consequence of closing inlet vent

Brady MANESCAU, Hui-Ying WANG, Jean Pierre GARO, Bruno COUDOUR and Lahna ACHERAR

wang@ensma.fr

Fax : 335 49 49 82 91

Institut P', Fluides-Thermique-Combustion, CNRS, ENSMA, Université de Poitiers, BP 40109
F86961 Futuroscope Chasseneuil Cedex, France

ABSTRACT

In the industrial environments, one of the ways to prevent the spread of harmful fire by-products to adjacent compartments via ventilation networks consists in applying an Inlet Valve Closure (IVC) procedure. A theoretical research by means of the experiments and the physics-based models is performed to investigate the consequences of closing air intake on fire behavior in the mechanically ventilated compartment. In well-ventilated conditions, the strategy of closing inlet vent can be considered as a positive factor with a reduction in HRR regardless of fuel type such as heptane or dodecane. In under-ventilated conditions, replacing heptane by dodecane with a higher boiling point leads to a change in fire dynamics regime from a ventilation to fuel controlled fire. Closing inlet vent contributes to a faster heptane fire growth with an increase in theoretical HRR by a factor of 5%, and however, exhaust of the ventilation controlled fire occurs more easily due to a reduction in combustion efficiency by a factor of 30%. However, for the dodecane fire, closing inlet vent facilitates a reduction in HRR over a longer burning period. Air entering the compartment follows closely the fluctuations of the fire induced pressure as a result of strong coupling process between drop in pressure and inlet flow rate. For the heptane fire in vitiated air environment, the impact of stopping inlet vent on the peak of unburnt species concentration seems negligible. Dodecane with a longer carbon chain produces more unburnt gases than heptane, and turning off air intake results in a reduction in unburnt species. Occurrence of flame extinction in the vitiated air enclosure makes a sudden supply of fresh air from dilution duct with an oxygen concentration of about 15%, ideal condition for triggering an eventual auto-ignition of a fuel-air mixture. With regarding the delay time for an ignition risk of unburnt pyrolyzates, the heptane fire appears more dangerous by closing inlet vent. For the dodecane fire, stopping inlet vent contributes to a prolongation in ignition delay time of unburnt pyrolyzates.

KEYWORDS:
enclosure fire, liquid fuel, drop in pressure, air intake, closing inlet vent, ignition risk, extraction duct, dilution

NOMENCLATURE LISTING

C_p	specific heat ($kJ.kg^{-1}.K^{-1}$)
D	diameter of liquid pan (m)
D*	characteristic length of pool fire (m)
Fr	Froude number
g	gravity ($m.s^{-2}$)
H_{eav}	Heaviside unit step function
L	characteristic length of enclosure (m)
L_v	pyrolysis heat
$\dot{m}_F$	mass loss rate of liquid fuel ($kg.s^{-1}$)
$\dot{m}_A$	inlet air flow rate ($kg.s^{-1}$)
P_0	atmospheric pressure (Pa)
P	enclosure pressure (Pa)
$\dot{q}''_{r,flame}$	radiation heat flux from flame ($kW.m^{-2}$)
$\dot{q}''_{r,smoke}$	radiation heat flux from smoke ($kW.m^{-2}$)
$\dot{q}''_{r,wall}$	radiation heat flux from wall ($kW.m^{-2}$)
$\dot{Q}$	heat release rate (kW)
$\dot{Q}_{the}$	theoretical heat release rate (kW)
$\dot{Q}_{eff}$	effective heat release rate (kW)
Re	Reynolds number
Sc_t	turbulent Schmidt number
T	temperature (°C)
T_f	flame temperature (°C)
T_m	bulk temperature (°C)
t	time (s)
u	velocity ($m.s^{-1}$)
V	volume of combustion zone or enclosure (m^3)
$\dot{V}_{max}$	maximum volume flow rate ($m^3.h^{-1}$)
$\dot{V}_{total}$	total volume flow rate ($m^3.h^{-1}$)
$\dot{V}_{admission}$	volume flow rate from admission duct ($m^3.h^{-1}$)
$\dot{V}_{dilution}$	volume flow rate from dilution duct ($m^3.h^{-1}$)
$\dot{V}_{leakage}$	volume flow rate from leakage ($m^3.h^{-1}$)
Y_{soot_yield}	soot yield
Y_n	mass fraction of chemical species, n
$Y_{O2,lim}$	critical oxygen concentration for extinction
x, y, z	coordinates system in numerical simulation

Greek

ρ	volume density ($kg.m^{-3}$)
τ_{mix}	key mixing timescale (s)
τ	flow time scale (s)
ν_i	stoichiometric coefficient (i=O_2, CO, H_2, soot)
$\dot{\omega}'''_n$	local reaction rate of chemical species, n
λ	thermal conductivity ($W.m^{-1}.K^{-1}$)

ϕ	global equivalence ratio
η	combustion efficiency
ΔP_{max}	maximum pressure difference (Pa)
ΔH_c	heat of combustion ($kJ.kg^{-1}$)
ΔH_o	energy released per kilogram of oxygen consumed (13100 $kJ.kg^{-1}$)

Acronym

ACPH	Air Change Per Hour (h^{-1})
AIT	Auto-Ignition Temperature (°C)
EDC	Eddy Dissipation Concept
GER	Global Equivalence Ratio
HRR	Heat Release Rate (kW)
HVAC	Heating Ventilation Air Conditioning
IVC	Inlet Valve Closure
LFL	Lower Flammability Limit (%vol)
MLR	Mass Loss Rate ($kg.s^{-1}$ or $g.s^{-1}$)
UFL	Upper Flammability Limit (%vol)

I. INTRODUCTION

Most residential and industrial buildings have multiple unprotected, glazed openings such as windows and doors to the external perimeter of the building. When a post-flashover compartment fire occurs in this type of building, and when the glazing falls out of these unprotected openings, an external flame plume is likely to occur due to limited ventilation conditions within the compartment. Different types of specialist installations, such as nuclear facilities, do not have these sources of ventilation, but rather rely exclusively on mechanical ventilation systems. In order to contain the potential release of radioactive material to the surrounding environment, nuclear facilities operate under negative pressure, known as dynamic confinement, relative to the ambient pressure external to the facility. The compartment fire dynamics in nuclear faculties are therefore very different to those typical in residential and industrial buildings. The combination of dynamic confinement, and the pressure build up induced by a fire, create unique fire hazards in nuclear installations relative to typical buildings [1]. The Pprime Institute and AREVA conduct a research programme on fire safety in nuclear installations on behalf of the French nuclear industry. Part of this ongoing research programme has several theoretical and experimental research projects that have investigated the unique fire safety hazards associated with nuclear facilities. This paper presents findings from a recent project that has focused on the fire dynamics in mechanically-ventilated compartments.

The impact of the physical compartment boundaries on the fire dynamics has been widely studied for several decades. A free-burning fire is almost unaffected by hot smoke in a downstream plume region as the temperature drops and more cold air is entrained. The physical compartment boundaries affect not only the combustion processes, but also the transport of thermal energy, reactants from the chemical reaction zones, and conductive heat loss to the walls. The example given in Fig.1 of a very large compartment could perhaps be described as a trend - as the compartment size increases, the trend is for surface/smoke layer radiation to have less influence [2]. Flashover is also linked to this, i.e. flashover is less likely to occur as the compartment size increases. Research [3] has demonstrated the compartment effects on degradation of liquid fuels into pyrolysis gases via the ceiling smoke radiation ($\dot{q}''_{r,smoke}$) and

walls radiation ($\dot{q}''_{r,wall}$). The large pyrolysis gas release is therefore something that may (or not) occur, depending on the situation so the fire may (or not) quickly become ventilation controlled. It is only as flashover is approached that noticeable enhancement of radiation heat feedback from smoke and walls will occur.

For a free-burning fire, air entrained from a predominant natural convection generates a self-sustaining flame in an almost steady burning up to burnout of the fuel. In a compartment, restricted ventilation impacts on fire behavior can be separated in several individual processes - during the initial phase, the fire grows as long as it is fuel-controlled; the amount of oxygen available for combustion limits the growth of the HRR compared to the unlimited ventilation case where the decay of the HRR occurs usually as the fuel is depleted; the fire may extinguish when oxygen concentration is lower than the minimum oxygen concentration of the burning fuel [4].

As a consequence of restricted ventilation, a compartment fire may produce consequent quantity of incomplete combustion products such as carbon monoxide and soot due to the inadequate oxygen [5]. The temporal evolution of oxygen, carbon dioxide and carbon monoxide during a compartment fire with ventilation has been extensively investigated [6]. The transport of unburnt gases from incomplete combustion would generally be to other parts of the building and the exterior where an ignition may occur in an oxygen available zone [7]. The accumulation of unburnt gases can create a flammable mixture that can ignite with an external ignition source or by self-ignition in ventilation networks [8], probably causing a fire propagation to adjacent compartments.

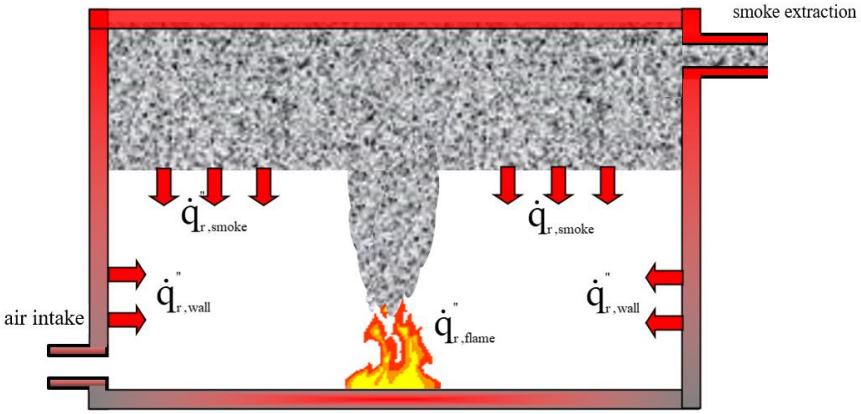

Figure 1. Scheme of heat feedback to a condensed fuel inside an enclosure fire

In nuclear facilities, one strategy to restrict fire development is the Inlet Valve Closure (IVC) procedure [9], i.e., limit the supply of fresh air into the compartment, thus restricting the available oxygen to that already in the compartment. Limiting the pyrolysis rate by fuel cooling with fire suppression agent, e.g., halon, is an alternative concept to restricting the fire development in the compartment of origin. However, application of this concept becomes difficult sometimes especially for a large-scale fire due to the uncontrollable heat feedback to condensed fuels. Closing the exhaust ducts generates a strong increase in pressure of the compartment fire to cause structural (or dynamic confinement) failure as well as a reverse flow in the supply ventilation system [10]. Applying the IVC strategy allows a significant reduction in HRR as a result of a restriction in air entering the compartment [10]. Current knowledge [9,

10] is considerably limited to the effects of closing the ventilation paths on fire development in well-ventilated conditions. This limitation is motivation of this theoretical research to look specifically the consequences of applying IVC procedure on the well- and under-ventilated compartment fires with various liquid fuels.

This project aims to discover if applying IVC procedure can be considered always as a positive factor in both fire growth rate and ignition risk of unburnt pyrolyzates due to limited oxygen. Liquids (mineral oil, synthetics, etc.) could originate e.g. from leaking transformers, generators or other machinery. Heptane has been widely used in compartment fire dynamics studies [8, 10] although this fuel is never used in nuclear facilities. Dodecane has a chemical formula similar to Hydrogenated Tetra-Propylene (HTP) which is a chemical solvent used in nuclear power plants. This study shows clearly the effects of different liquids such as heptane and dodecane on the fire duration, the HRR, the gas temperature and the species concentration as a consequence of applying IVC procedure. Since the decision making process regarding fire safety in nuclear facilities depends increasingly on numerical simulations, the experimental data are also used for assessment of FDS6.5 [11]. Although the CFD modelling was done after (a posteriori) the experiments, different modelling parameter values were not tried in order to get a better match to the experimental results. When the experimental data was compared to FDS6.5 calculations, in some cases the models validity was confirmed, while in other cases, the model did not predict the experimental results very well.

II. EXPERIMENTAL SET-UP

A schematic 3D view of the experimental facility in multi-scales with volume sizes of 0.4, 1, 8 and 15 m^3 is illustrated in Fig.2. Based on the dimensionless variable of energy equation, the source term contains a Zukoski number [12], defined as :

$$Zu = \frac{\dot{Q}}{Fr\, L^{5/2}\, (\rho C_p T)_\infty\, g^{1/2}} \qquad (1)$$

Here, ∞ denotes the ambient thermo-physical properties. The effects of the ratio, $\dot{Q}^2/L^5$, in Eq.(1) on fire dynamics regime was checked [13] in such type enclosure (cf. Fig.2), and a threshold value of about 13 is determined to identify well- or under-ventilated fires. In the current work, the compartment is a cube (8 m^3) with a characteristic length of L=2 m. Froude number of $Fr \approx 0.05$ and Reynolds number of $Re \approx 2x10^4$ are estimated from the measured inlet velocity after igniting the fuel pan. When conducting such reduced scale experiments, the well- and under-ventilated fires can be dealt with by regulating HRR, $\dot{Q}$, from 20 to 200 kW via the fuel pan size, corresponding approximately to a Zukoski number from 0.06 to 0.6. In general, the stratification of the smoke layer near the ceiling is more efficacious in the vertical direction to generate a change in fire dynamics regime. For a given enclosure volume, the height affects significantly the smoke establishment, and thus, it can be considered as the characteristic length if the compartment dimensions are not the same.

The enclosure is equipped with an external ventilation system. The air intake was placed in low position at a height of 0.3 m. The burnt gases flowed towards the extraction duct with a length of 1.1 m at a height of 1.7 m. The dilution duct with a length of 2.5 m is fixed at the same height. All the ventilation ducts have a square section of 0.2x0.2 m^2, and are made of smooth galvanized steel. The enclosure walls are made of 20-cm-thick cellular concrete which is a lightweight cement-based material, containing many gas bubbles evenly distributed in the volume. Cellular

concrete with λ=1 W/m/K, ρ=400 kg/m^3 and C_p=0.88 kJ/kg/K is used especially when chemical and fire resistance is needed. The measurements taken include MLR, velocity, pressure, temperature and chemical species concentrations of gases filling the enclosure.

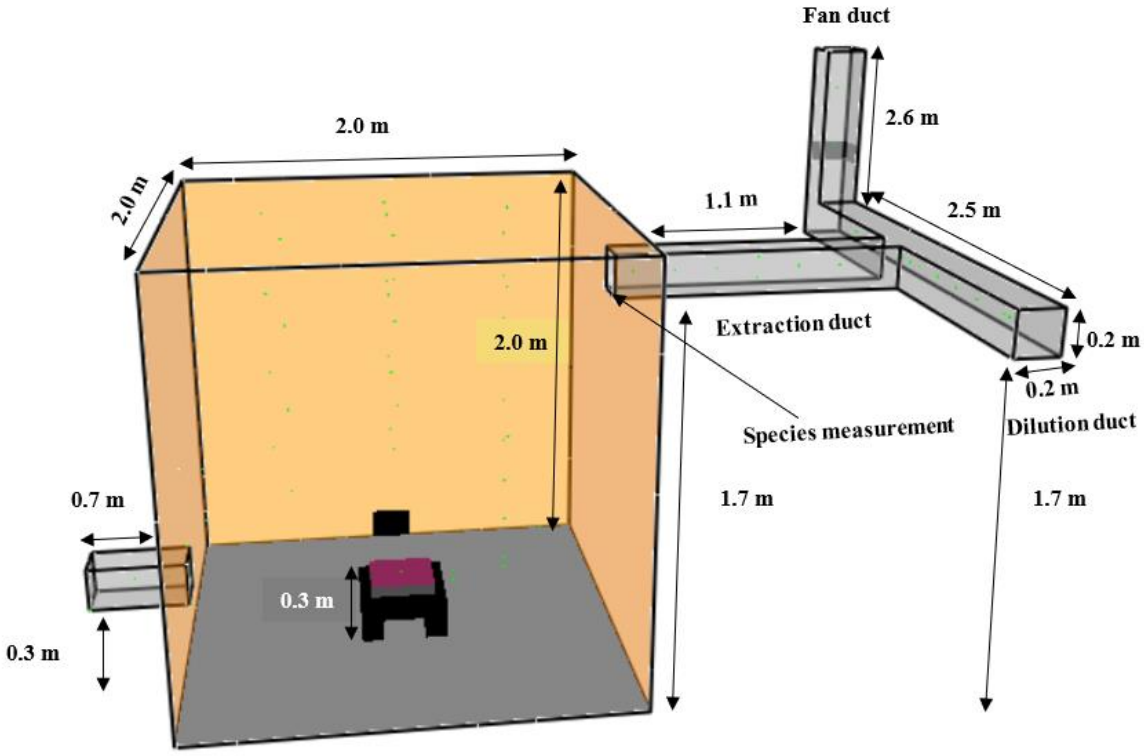

Figure 2. Scheme of the experimental set up consisting of a mechanically ventilated enclosure fire with interconnecting ventilation system

The air flow rates at the intake and the dilution ducts are regulated as a function of drop in pressure by means of an adjustment of rectangular flaps located upstream of these ducts, allowing to generate aeraulic resistances. The flow velocity in the inlet and the dilution ducts is measured by using a stainless steel hot wire probe placed at the entrance of these ducts with an uncertainty of ±0.3%.

As shown in Fig.2, to select the desired airflow rate, a centrifugal fan with single-phase variable speed is placed at the outlet of a duct orthogonal to the dilution duct at a height of 2.6 m. Such a mechanical extraction provides a maximum volume flow rate of $\dot{V}_{max} = 720$ m^3/h, and pressure difference of $\Delta P_{max} = 186$ Pa. The fan characteristic curve (i.e., delivered flow rate as a function of pressure) is shown in Fig.3.

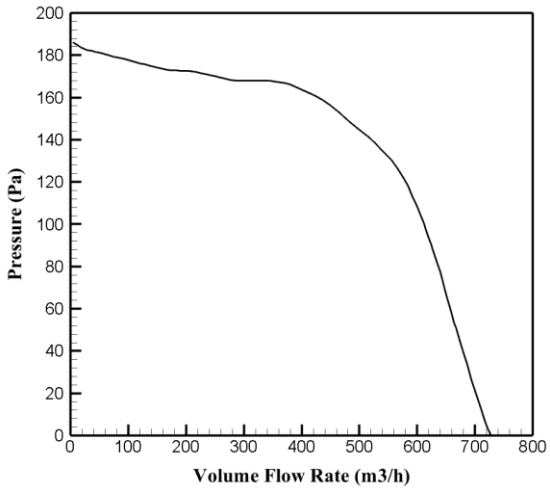

Figure 3. Relationship between pressure and free volume flow rate of the fan

Before igniting the fuel pan, a period of 10 minutes was included for establishing a drop in pressure which is measured continuously by a pressure sensor with a sensitivity of ± 2 Pa. Air entering the compartment is regulated as a function of drop in pressure which creates a suction effect from admission ($\dot{V}_{admission}$) / dilution ($\dot{V}_{dilution}$) ducts and leakage ($\dot{V}_{leakage}$). As the method used in nuclear installations, only in absence of the fire, a certain number of ACPH is achieved from the measured volume flow rate (m^3/h) at admission duct, defined as :

$$ACPH = \frac{\dot{V}_{admission}}{V} (h^{-1}) \quad (2)$$

With the air inlet open, air entering the compartment is expressed as :

$$\dot{V}_{total} = \dot{V}_{admission} + \dot{V}_{leakage} + \dot{V}_{dilution} \quad (3)$$

After igniting the fuel pan, air entering the compartment is connected with the pressure variations which are based on a drop in pressure regulated initially at a certain number of ACPH in absence of the fire. By applying IVC procedure ($\dot{V}_{admission} = 0$) as soon as the fire starts, air initially present in the compartment and air entering the compartment from leakage and dilution duct via a drop in pressure become the primary source of ventilation for the fire development.

$$\dot{V}_{total} = \dot{V}_{leakage} + \dot{V}_{dilution} \quad (4)$$

The dilution duct in effect becomes a secondary air inlet especially at fire extinction point due to a significant drop in pressure as a counter-flow in the extraction duct (cf. Fig.2), resulting in a sudden increase of oxygen concentration in the ceiling smoke layer.

According to our experimental observation, as a consequence of a restriction in air entering the compartment at a low ACPH, the phenomena of periodic oscillations with flame presence/absence nearby the fire source generate large variations in pressure peak. Fires performed at a high ACPH induce strong oscillations of HRR due to the enhanced turbulence effects on fire development, and as a result, large amplitudes of pressure especially in the case of closing air intake. When many enclosure fire tests were undertaken, structural failure of the experimental set-up seems probable as a consequence of large variations in pressure peak. On the other hand, in the nuclear installations, ACPH is often limited to 5 with a moderate drop in pressure. For the current enclosure fire tests, only 3 and 5 ACPH are considered.

The gas temperature measurement were taken at entrance of the extraction duct with chromel-alumel thermocouples (type K) of a 0.5 mm wire. Globally, uncertainty in the measurement of gas temperature could originate from the thermocouple response to conversion of the flame or the gas temperature in digital signal. In fire environment with an accumulation of soot particles and reactions, a radiation correction is necessary to ensure the accuracy of flame temperature measurement due to the radiation heat exchanges from thermocouples to the exterior. Besides, the flame temperature variation is related to the thermocouple diameter via convection, and a decrease in diameter of the thermocouple causes a reduction in flame temperature. By taking into account the above potential errors, including thermal mass inertia, soot particles, surface reactions, radiation, convection and thermocouple diameter, uncertainty in the measurement of gas temperature by using thermocouples is estimated within 5% [14].

Local continuous measurement of molar fraction of oxygen at the extraction duct was taken by using a sampling probe. A No-Dispersive Infrared gas analyzer was used to follow the evolution of CO and CO_2 concentrations, and a paramagnetic gas analyzer to follow the evolution of O_2 concentration. Hydrogen concentration as well as concentrations of hydrocarbons that have a carbon chain length lower than or equal to four are measured by ten sampling probes, following the same methodology as carbon monoxide concentration measurements. A sample is analyzed with a time lag which can be estimated between 60 and 80 s depending on the test, thus generating a gap between HRR and oxygen concentration.

The fuel was burned in a circular stainless steel pan with a depth of 5 cm, and the quantity of fuel used was 0.75, 1.67 and 3.4 kg, respectively for pan diameter of 23, 30 and 40 cm. Liquid fuel pan was placed in the middle of the enclosure, slightly elevated at a height of 0.3 m. MLR of the liquids such as heptane and dodecane was measured by a loadcell which was positioned under the pan. The load cell has a response time of 60 ms with an uncertainty of measurements within ±5%.

III. NUMERICAL MODELLING

Based on the geometry shown in Fig. 2, FDS6.5 [11] was used to replicate and model the experiments. This section provides only a summary of the physics-based model utilized in the current work.

A reaction mechanism via three sequential, semi-global steps [15] is considered for taking into account incomplete combustion products during a fire.

$$\left.\begin{aligned} &\text{i)}\ C_x H_y + \nu_{O2} O_2 \rightarrow \nu_{CO} CO + \nu_{H2} H_2 + \nu_{soot} C_{soot} \\ &\text{ii)}\ CO + \frac{1}{2} O_2 \rightarrow CO_2 \\ &\text{iii)}\ H_2 + \frac{1}{2} O_2 \rightarrow H_2O \end{aligned}\right\} \qquad (5)$$

The turbulent combustion processes are assumed to be governed by the conservation equations between transport and production for mass fraction of the following major chemical species such as C_xH_y, O_2, CO, H_2, C_{soot}, CO_2 and H_2O.

$$\frac{\partial \rho Y_n}{\partial t} + \frac{\partial [\rho u_i Y_n]}{\partial x_j} - \frac{\partial}{\partial x_j}\left(\frac{\mu_t}{Sc_t} \frac{\partial Y_n}{\partial x_j} \right) = \dot{\omega}_n''' \quad (6)$$

Here, the x_j represents the j^{th} direction in the spatial coordinate. The turbulent Schmidt number, Sc_t, is assumed to be constant with a value of 0.5 [11] (Section 6.4.8).

The local turbulent reaction rate is calculated from an Eddy Dissipation Concept (EDC) [11] (Section 12.1.3), as follows :

$$\dot{\omega}_n''' = -\frac{\rho}{\tau_{mix}} \min(Y_n, \frac{Y_{O2}}{s}) \cdot H_{eav}(Y_{O2} - Y_{O2,lim}) \quad (7)$$

Here, the n denotes the primary fuel (C_xH_y), CO and H_2. The key mixing timescale in Eq.(7), τ_{mix}, is supposed to relate approximately to the three processes of diffusion, subgrid-scale advection and buoyant acceleration. The source term in Eq.(7) is multiplied by $H_{eav}(Y_{O2}-Y_{O2,lim})$ which is zero when its argument is negative ($Y_{O2}<Y_{O2,lim}$) and 1 when it is positive ($Y_{O2}>Y_{O2,lim}$). Flame extinction occurs as the local oxygen concentration is below a critical value, $Y_{O2,lim}$, which is evaluated as a function of specific heat (C_p), flame temperature (T_f) and bulk temperature (T_m) [11] (Section 12.1.4).

$$Y_{O2,lim} = \frac{C_p(T_f - T_m)}{\Delta H_o} \quad (8)$$

Soot formation rate, $\dot{\omega}_s'''$, in Eq.6 is derived from a simple soot conversion model [11] (Section 12.4) :

$$\dot{\omega}_s''' = -\nu_{soot} \dot{\omega}_{CxHy}''' \quad (9)$$

The stoichiometric coefficient, ν_{soot}, is derived from the fraction of fuel mass that is converted into soot, y_{soot_yield} :

$$\nu_{soot} = \frac{W_F}{W_S} y_{soot\_yield} \quad (10)$$

Here, W_F and W_s denote the primary fuel (C_xH_y) and soot molar weights, respectively. The stoichiometric coefficients, $\nu_{O2}, \nu_{CO}, \nu_{H2}$, in the reaction mechanism (cf. Eq.5) are also determined from the chemical formula of the primary fuel [11] (Section 12.2.1).

For a sooting flame as heptane or dodecane pool, soot production controls the thermal radiation from the flame and hot smoke. The simplifying assumption is made that the gas is gray, and one absorption coefficient without the spectral dependence is employed in a radiation transfer equation [11] (Section 13). A one-dimensional heat transfer equation for the material temperature is solved using a finite difference method. The size of the mesh cells on the surface of the wall is automatically chosen using a rule that makes the cell size smaller than the square root of the material diffusivity $(\lambda/\rho C_P)$. By default, mesh cells of the condensed phase increase towards the middle of the material layer and are smallest on the layer boundaries. The numerical accuracy and stability of the condensed phase solution can be improved by reducing the cell size [11] (Section 8.3.8). The thermo-physical and combustion properties [15] of heptane and dodecane used in the numerical simulations are provided in Table 1.

Table 1. Thermo-physical and combustion properties of heptane and dodecane

Property	Heptane	Dodecane
Conductivity, λ (W/m.K)	0.17	0.14
Density, ρ (kg/m^3)	684	750
Specific heat, C_p (kJ/kg.K)	2.24	2.21
Pyrolysis heat, L_v (kJ/kg)	321	256
Heat of combustion, ΔH_c (kJ/kg)	44500	44147
Boiling temperature T_b (°C)	98	216
Flash point (°C)	-4	74

A dedicated module for modelling Heating, Ventilation and Air-Conditioning (HVAC) systems, consisting of mass, energy and momentum equations, is coupled with the gas phase solver. Fan is included in the HVAC network, and its resulting volume flow rate can be determined from a basic quadratic formulation which is a module in FDS6.5 [11] (Section 9.2.4) based on a fan characteristic curve as shown in Fig.3.

The enclosure envelope is not perfectly air tight, providing small paths through obstructions. In non-fire condition, a difference in the volume flow rates between the inlet and the extraction ducts due to leakage is experimentally detected with an average value of $\dot{V}_{leak} \approx 0.02$ m^3/s. The relation between leakage volume flow rate and area as a function of the pressure difference can be described as follows :

$$\dot{V}_{leak} = A_L \, \mathrm{sign}(\Delta P) \sqrt{2|\Delta P| / \rho_\infty} \qquad (11)$$

By using Eq.(11), the total leakage area, A_L, from the gaps around door and enclosure construction as well as passage of the thermocouples is estimated in the order of 15 cm^2 with a drop in pressure, ΔP, of about 100 Pa. From the viewpoint of fire CFD, since leakage is a sub grid-scale phenomenon, a leak path boundary condition can't be directly specified. In FDS6.5 simulations [11] (Section 9.3.2), the leaks are modelled through the HVAC module as a finite area, A_L, using vents on the domain boundaries via the leakage flow velocity, $u_{leak} = \dot{V}_{leak} / A_L$ (m/s). The influence of the leakages for this set-up has been examined by using FDS6.5 [11]. It is found that after activating the fire, oscillation of the pressure difference between the inside and the outside induces a leakage flow velocity of about 13 m/s by using a small leakage area of 15 cm^2. Such a strong air jet significantly disturbs the pool fire if the leakage area is located in low position, or the smoke layer near the ceiling if it is in high position. However, the experimental results show no disturbance of fire or smoke layer by leakage flow. Since we lack the ability to identify the leakage locations (door, passage of the thermocouples, etc.), the bulk leakage method [10] which refers to the amount of air flowing through the enclosure envelope, is used. The simplifying assumption is made that leakage does not directly participate in the ventilation of the fuel pans.

In a Large Eddy Simulation, turbulence is modelled using a Deardorff's approach [11] (Section 6.4.8) via subgrid viscosity which is attached to the grid size. More work on verification and validation of selected fire models [16] indicated that the large-scale energy-containing eddies are completely described when the characteristic length is spanned by roughly sixteen computational cells. Following this viewpoint [16], the layered structure of the smoke in full-scale enclosure fires [17] was successfully captured with a mesh of 10 cm. For this set-up, a proper cell sensitivity analysis was performed on the calculated quantities in the previous work [18]. It is found that *a priori* estimates of the mesh size of 5 cm with the same criterion [16] seems to be enough to reach a grid convergence for the calculation of the fluid motion outside the flame zone. An extremely small grid size of about 1 mm to fully resolve the characteristic flame thickness would have made practical fire simulations difficult. By using 16 processors through parallel processing of a Linux cluster, the CPU time for a simulation with a physical time of about 2500 s is approximately 24 h.

IV. RESULTS AND DISCUSSION

The experiments and the modelling were carried out for a series of 16 different scenarios with variations in pan size (D), ACPH, air intake and fuel type, as described in Table 2. The attempt to predict MLR of liquid pool fires by using FDS6.5 in a vitiated air enclosure was not successful [17]. The surface tension gradients resulting from temperature gradients at surface of liquid pool fires are likely to be important [19]. In FDS6.5 (Section 8.3.8), since liquid is treated as a solid, the effects of heated liquid-phase flow due to the surface tension gradients on MLR can't be taken into account. Currently, the existing empirical correlations [20] for liquid burning can't again reproduce the strong perturbation of MLR in a vitiated air enclosure. Due to lack of the ability to properly calculate MLR of liquid pool fires, the non-predictive simulations were performed in the current work. The fire boundary condition was prescribed by the experimental MLR curves over the surface of the liquid fuel. We focus on the analysis of the fire growth rate as well as on the resulting pressure, the velocity, the species and the gas temperature in transient mode.

Table 2. Experiments and simulations conducted fire scenarios

Fire scenarios	Pan size, D (cm)	ACPH (h^{-1})	Air intake	Fuel type
1	23	3	opening	heptane
2	23	3	closing	heptane
3	23	5	opening	heptane
4	23	5	closing	heptane
5	30	3	opening	heptane
6	30	3	closing	heptane
7	30	5	opening	heptane
8	30	5	closing	heptane
9	30	3	opening	dodecane
10	30	3	closing	dodecane
11	30	5	opening	dodecane
12	30	5	closing	dodecane
13	40	3	opening	dodecane
14	40	3	closing	dodecane
15	40	5	opening	dodecane
16	40	5	closing	dodecane

IV.1 Repeatability of the tests

For each compartment fire, three tests are taken to check repeatability of MLR of the liquid fuels. It is found that repeatability of the tests depends on fire dynamics regime which can be characterized by a Global Equivalence Ratio (GER), defined as $\phi = \dot{m}_F \nu / \dot{m}_A$. An empirical relationship [21] is established to evaluate the level of air vitiation nearby the fire source from the measured oxygen concentration in smoke layer near the ceiling, as

$$X_{O2,\,floor} \approx 0.8 X_{O2,\,ceiling} + 0.07 \text{ for } X_{O2,\,ceiling} \in [0.05,\ 0.17] \qquad (12)$$

The Bryner's work [22] indicated that oxygen concentration above 15% corresponds to a well-ventilated fire with GER below 0.7. The range of oxygen concentration between 10% and 15% implies an under-ventilated fire with GER between 0.7 and 1. Oxygen concentration below 10% translates to a fire exhaust close to extinction with GER above 1.

The fire scenarios 3, 7 and 13 are considered to illustrate the repeatability of liquid MLR. For the heptane experiment of 23 cm (cf. Fig.4a, scenario 3), oxygen concentration nearby the fire source is estimated from Eq.12 with a value of 15%, corresponding to a well-ventilated fire. A good repeatability was obtained with an average variation in MLR of ±0.15 g/s. When a liquid fuel is subjected to a heat flux from a torch, the surface temperature of liquid increases and liquid starts releasing flammable gas. Ignition of the heptane pan has been pretty much instantaneous when using a torch due to its lower flash point (cf. Tab.1). However, with about 30 and 50 s respectively for the dodecane pan of 30 and 40 cm, concentration of the dodecane which is immersed into the gas phase increases subsequently passing a lean flammability limit for ignition. The ignition phase and perturbation of air entering the compartment have an influence on the peak value of MLR. The variability of ±50 s in extinction time due to fuel burnout depends on the peak value of MLR. A low peak value results in a longer burning period, and inversely, a high peak value conducts to a reduction in the decaying phase delay. The heptane experiment of 30 cm (cf. Fig.4b, scenario 7) conducts to an under-ventilated fire due to a rapid fall of oxygen concentration to about 5% nearby the fire source (cf. Eq.12). The repeatability of scenario 7 (cf. Fig.4b) seems better for the first 200 s with very consistent growth peak and decay, but it is only after 200 s that the worst repeatability occurs. Starting from 200 s, the oxygen starvation begins, and the oscillating flame close to extinction becomes more perturbed. This conducts to a maximum variation in MLR of ±0.65 g/s between the three tests. A deviation of the fire extinction delays exceeds ±100 s between the tests 1 and 2, and up to ±250 s between the tests 1 and 3. The dodecane experiment of 40 cm (Scenario 13, cf. Fig.4c) is identified as an under-ventilated fire, translating to a maximum variation in MLR of ±1 g/s, and a deviation of ±200 s in the fire extinction delays between the three tests.

Repeatability of the fire dynamics regime depends on GER, and the GER of 0.7 can be considered as the indicative threshold between a well- and under-ventilated fires. A well-ventilated fire $(\phi \leq 0.7)$ is relatively stable, and a good repeatability of the fire dynamics regime can be obtained. Repeatability of the fire dynamics regime is degrading as long as the fire is ventilation controlled $(\phi > 0.7)$ due to an uncontrollable oscillation of the flame.

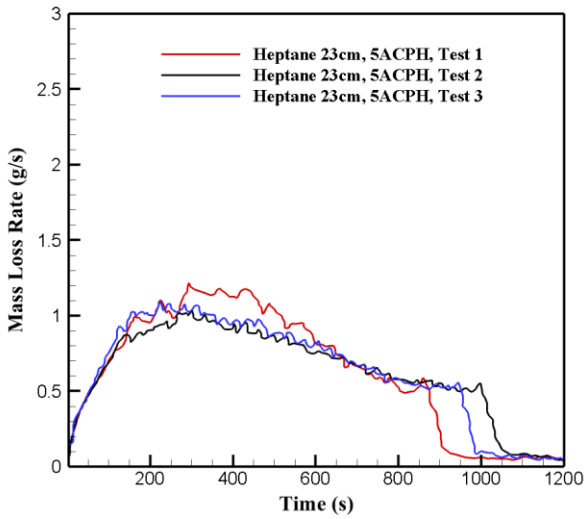

4a) Fire scenario 3

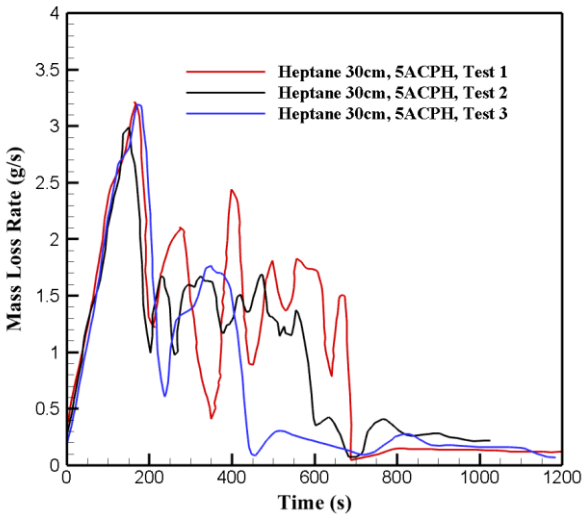

4b) Fire scenario 7

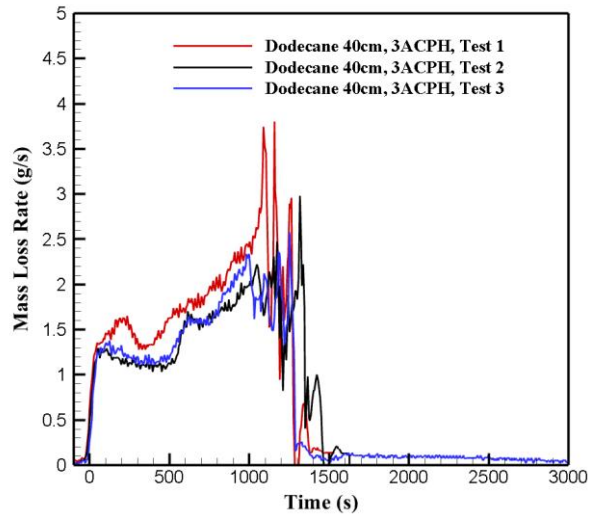

4c) Fire scenario 13

Figure 4. Repeatability of MLR with the three tests for the fire scenarios 3, 7 and 13

IV.2 Effect of the soot yield values on a free buoyant reacting plume

In FDS6.5 [11] (Section 12.4), a simple soot conversion model is used via a soot yield value (cf. Eqs.9, 10) which can be experimentally determined only in well-ventilated conditions, e.g., 0.037 for heptane and 0.047 for dodecane [23]. Such soot yield approach does not incorporate the essential physical processes of soot inception, coagulation, surface growth and oxidation in addition to the influences of turbulent fluctuations and temperature [24]. It is well known that the soot yield is influenced by the air vitiation level inside an enclosure [5] as a function of ventilation conditions.

The objective of this section is to assess the importance (or not) of the soot yield value in calculation of the gas temperature and the radiant heat flux over liquid surface. The radiant heat flux over liquid surface was measured by means of Gardon-gauge-type radiometer MEDTHERM which is equipped with a window to eliminate the conductive and convective

components from the flame. A detailed description of the measurement method on the radiant heat flux is given in our previous work [18]. The heptane experiment of 23 cm outside the compartment is chosen because the deduced radiant heat flux at the liquid surface is acceptable with an uncertainty of about 20% for an almost steady burning. Such a free buoyant reacting plume gives a steady MLR of 0.85 g/s (about 36 kW) instead of a peak value of 1.2 g/s (cf. Fig.4a) for the compartment fire with smoke/walls radiation. The attempt was not successful for the under-ventilated fires with the measured exaggerated spikes of radiant heat flux at liquid surface due to a strong perturbation of the flame.

The gross structure of a buoyant heptane fire is described in Fig.5 through the measured temperature contours by using thermocouples. The numerically computed temperature contours (cf. Fig.5b, c) are compared with the experimental measurements (cf. Fig.5a) for the soot yield values of 0.037 and 0.065. The overall visual temperature distribution exhibits a difference between the experimental data (cf. Fig.5a) and the calculations (cf. Fig.5b, c) regardless of the soot yield value. The comparison of the predicted and the measured temperature profiles at different radial locations (R=0, 3, 6, 9, 10.5 cm) is shown in Fig.6. Overall, the prediction of axial profiles at R=0 is in relatively good agreement with the experimental data. A low soot yield value of y_{soot_yield}=0.037 results in an increase of the gas temperature at axial locations, and inversely, more soot with y_{soot_yield}=0.065 conducts to a decrease of the gas temperature due to an increase of the radiation loss. Near the leading edge (R=6, 9, 10.5 cm), the magnitude of the gas temperature from the numerical simulations is substantially lower in comparison with the experimental data regardless of the soot yield value.

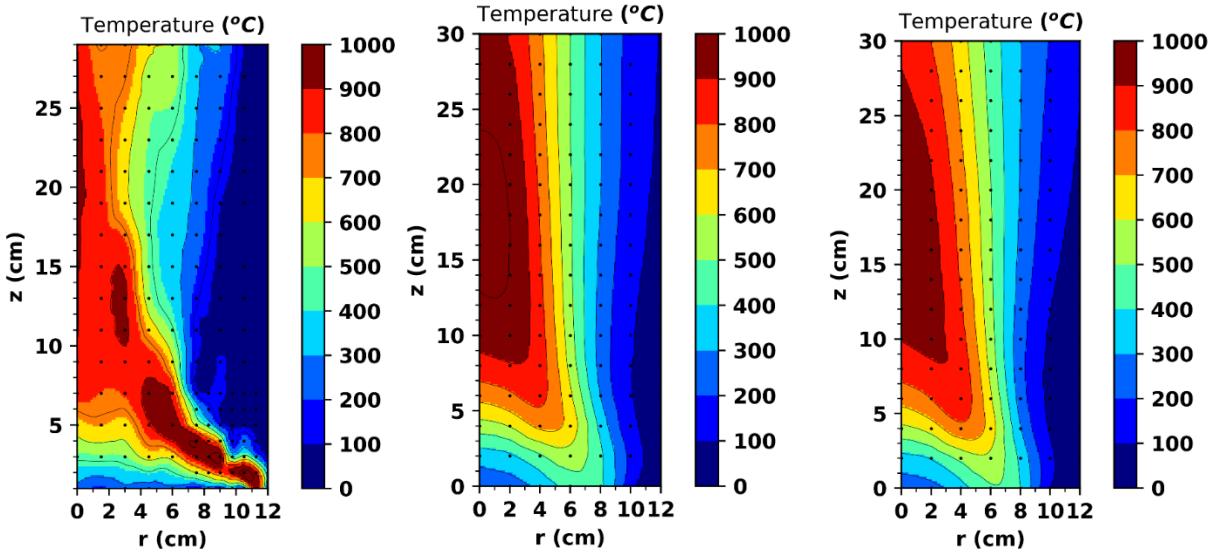

5a) Experiment 5b) y_{soot_yield}=0.037 5c) y_{soot_yield}=0.065

Figure 5. Comparison between the experimental data and the calculated temperature contours with two soot yield values

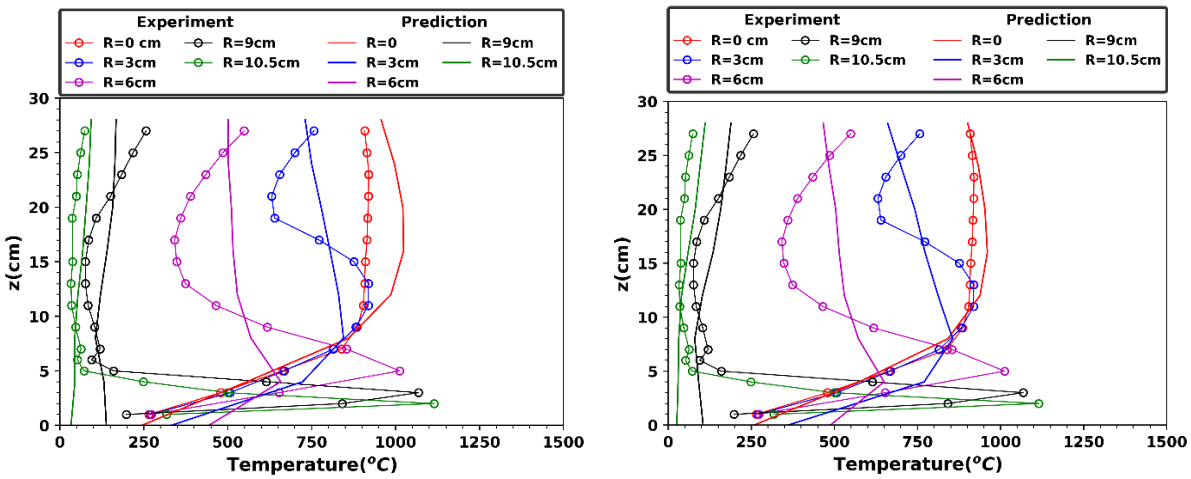

6a) Profiles with y_{soot_yield}=0.037 6b) Profiles with y_{soot_yield}=0.065

Figure 6. Comparison between the predicted and the measured temperature profiles at five radial locations (R=0, 3, 6, 9 and 10.5 cm) for two soot yield values

Fig.7(a, b) shows contours of the calculated soot volume fraction (ppm) for this heptane diffusion flame with two soot yield values. It is found that the maximum soot is numerically reproduced just above the fuel surface where the fuel-air mixture is relatively cool and rich in fuel. Physically, heat is released above this fuel-rich core as the fuel reacts with the entrained air, yielding combustion products as CO, CO_2 and soot. In a downstream plume region, soot decreases progressively as the gas temperature drops and more cold air is entrained. The calculations show an increased peak in soot volume fraction and an elongated higher soot formation region with an increase of soot yield value from 0.037 to 0.065.

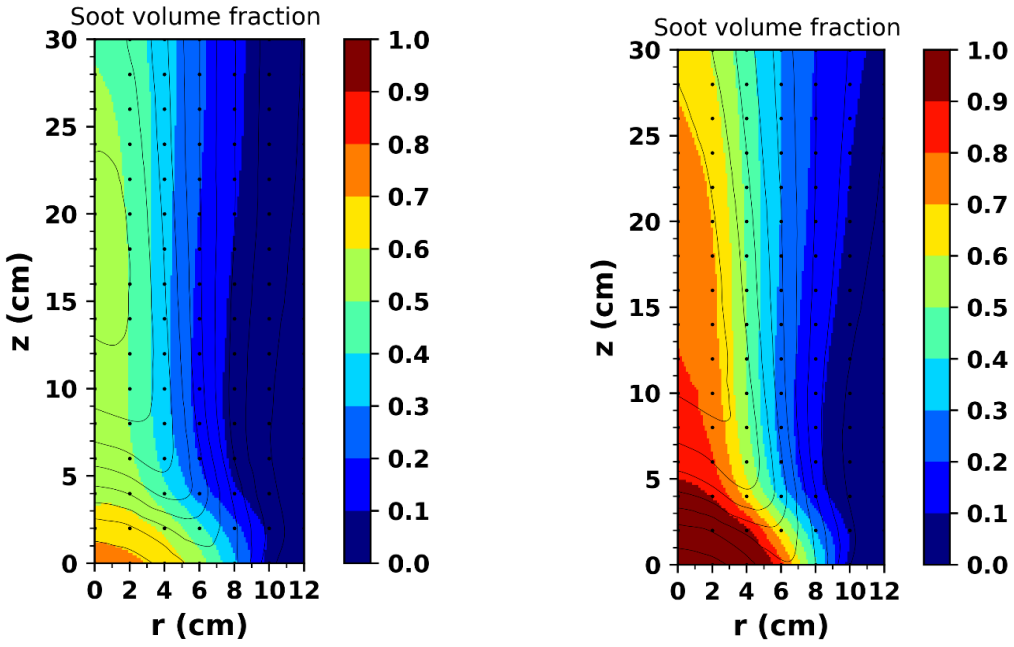

7a) y_{soot_yield}=0.037 7b) y_{soot_yield}=0.065

Figure 7. Effects of the soot yield value on contours of the calculated soot volume fraction (ppm)

The radiant heat flux at the liquid surface is a function of both the gas temperature with T^4 dependence, and the concentrations of gaseous/particulate soot emitting species. As shown in Fig.8(a, b), an overestimate of the radiant heat flux at the liquid surface is mainly attributed to a larger soot formation in the fuel-rich core (cf. Fig.7) regardless of the soot yield value. Globally, with multiplying the soot yield value by a factor of 2, the peak in radiant heat flux increases by a factor of 10%.

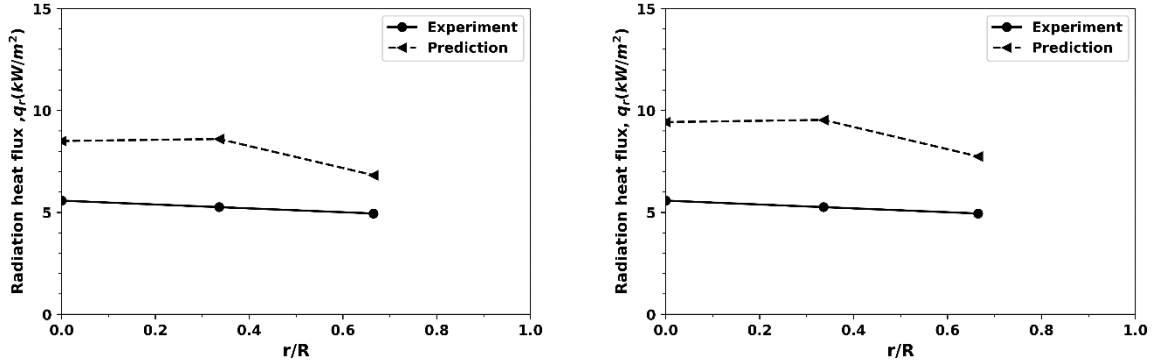

8a) y_{soot_yield}=0.037 8b) y_{soot_yield}=0.065

Figure 8. Comparison between the predicted and the measured radiant heat fluxes at liquid surface for two soot yield values

It is believed that a deviation in calculation of the gas temperature and the radiant heat flux over the liquid surface is not solely due to errors induced by a soot yield value. Rather, it is associated with uncertainties in other modelling aspects, such as subgrid diffusion and combustion models under laminar-like conditions in the fuel-rich core and near the leading edge. In addition, neither of the gas temperature and the soot can be reliably calculated in fire simulations even in a reduced-scale because the flame sheet can't be well-resolved on a relatively coarse grid with a size of cm. In the following numerical simulations, the soot yield values of heptane and dodecane in well-ventilated conditions are approximately used.

IV.3 Fire dynamics in confined compartment

The theoretical HRR is derived from the measured MLR ($\dot{m}_F$), e.g., in Fig.4.

$$\dot{Q}_{the} = \dot{m}_F \Delta H_c \quad (13)$$

In under-ventilated conditions, the whole vaporized fuel is not burnt instantaneously, thus Eq.(13) is likely to overpredict HRR. For the experiments reported in this paper, we did not have the necessary equipment to be able to use oxygen consumption calorimetry [25] to predict HRR. The effective HRR is estimated from the measured oxygen concentration, e.g., in Figs.10 and 13, at entrance of the extraction duct, as follows :

$$\dot{Q}_{eff} = \dot{m}_A (Y_{O2,\infty} - Y_{O2}) \Delta H_O \quad (14)$$

Concept of the limited ventilation affecting combustion efficiency is taken into account via the ratio between the effective (Eq.14) HRR and the theoretical one (Eq.13), expressed as $\eta = \dot{Q}_{eff} / \dot{Q}_{the}$.

Impact of the fuel type on the temporal evolution of HRR as a consequence of applying IVC procedure is analyzed in Fig.9(a-d) for the heptane experiments of 23 cm (scenarios 1-4). Note that the fire regime of the dodecane experiments of 30 cm (scenarios 9-12) is equivalent to the one of the heptane experiments of 23 cm (scenarios 1-4). The measured and the calculated

oxygen concentrations near the extraction duct are presented in Fig.10(a, b) for the corresponding fire scenarios. From Eq.(12), oxygen concentration nearby the fire source (floor) is estimated with a value of 15% when $X_{O2,ceiling}$ decreases to about 10% (cf. Fig.10) even by closing air intake. Fig.9(a-d) shows that the compartment fire scenario can be said to follow the four main stages, such as incipient, growth, fully developed and decay phases. After the incipient stage during about 10 s, the growth stage corresponds to a sharp rise of HRR, and the fully developed stage is reached with a maximum HRR (cf. Fig.9a, c). This is followed by a fire decaying phase with a slow decrease of HRR even if it remains fuel in the pan because oxygen initially present in the compartment (8 m^3) is consumed. The effective HRR (Eq.14) corresponds approximately to the theoretical HRR (Eq.13) with GER lower than 0.7, implying a well-ventilated fire with a combustion efficiency close to unity. Air entering the compartment from the admission duct allows to bring more oxygen nearby the pool fire. The magnitude of HRR is enhanced to a value of 53 kW at 5 ACPH (cf. Fig.9c) instead of 35 kW at 3 ACPH (cf. Fig.9a). Applying IVC procedure generates a slight increase in magnitude of HRR from 30 to 35 kW, that is to say by a factor of 10%, with an increase of ACPH from 3 to 5 (cf. Fig.9b, d). The strategy of applying IVC procedure can be considered as a positive factor in a reduction of the maximal HRR by a factor of 30%, but as a negative factor with regarding a prolongation in the fire duration by a factor of 40%. Usually, a low peak in HRR at 3 ACPH results in a longer fire duration. Extinction of a well-ventilated fire due to burnout of liquid fuel conducts to a rise of oxygen concentration (cf. Fig.10). The calculated oxygen concentration is with an error below 2% in comparison with the measured one. The HRR reproduced by the oxygen limited combustion model (Eq.7) follows closely the measured HRR with a good accuracy.

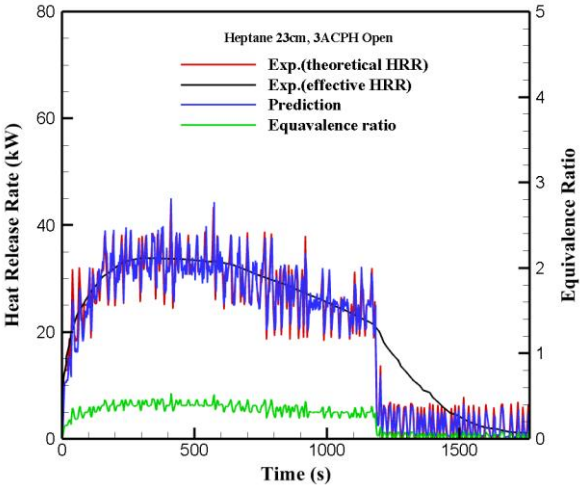

9a) Fire scenario 1

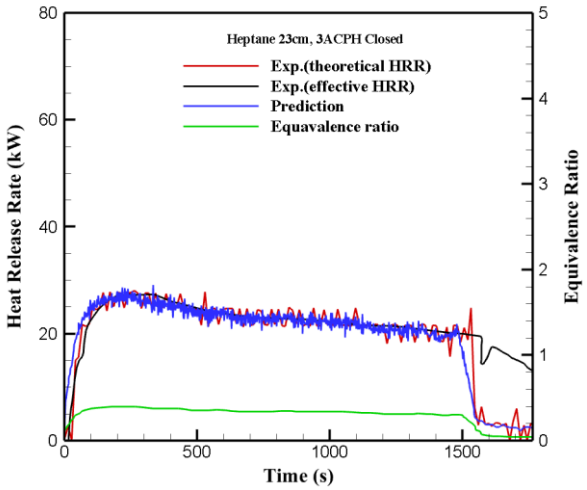

9b) Fire scenario 2

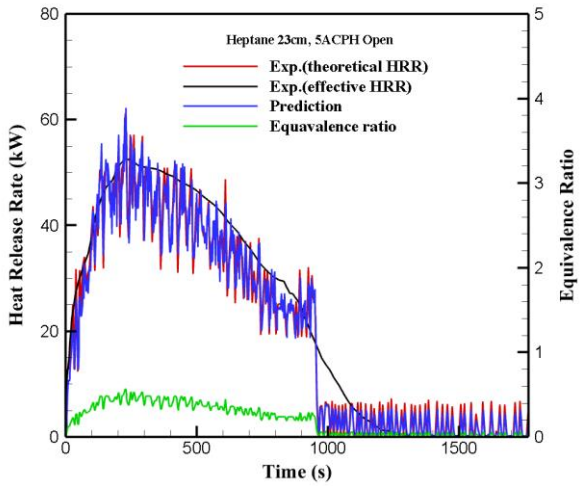

9c) Fire scenario 3

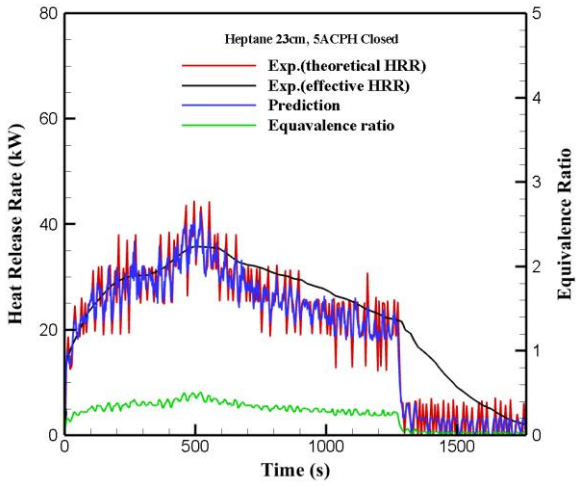

9d) Fire scenario 4

Figure 9. Impact of stopping air admission on HRR for the heptane pan of 23 cm in well ventilated conditions

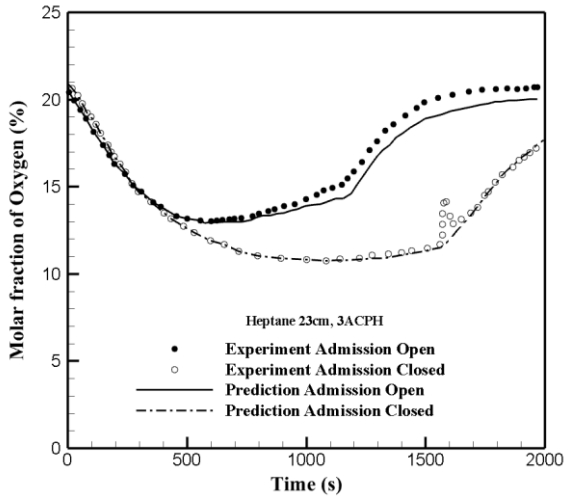

10a) Fire scenarios 1-2

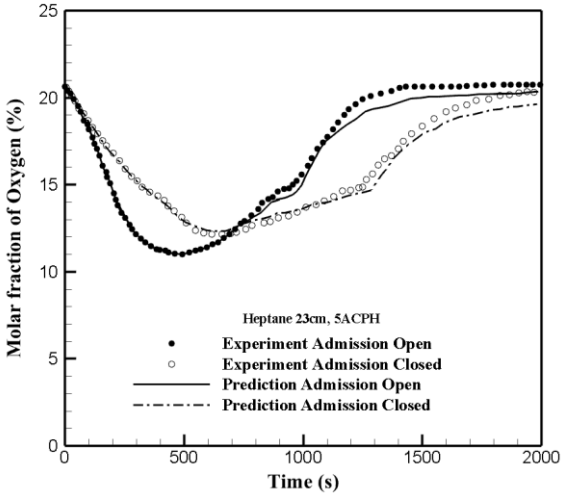

10b) Fire scenarios 3-4

Figure 10. Impact of closing air intake on the time history of oxygen concentration for the heptane pan of 23 cm in well ventilated conditions

The heptane experiments of 30 cm (scenarios 5-6) and the dodecane experiments of 40 cm (scenarios 13-14) correspond to under-ventilated fires with GER higher than unity. The temporal evolutions of HRR and oxygen concentration at 3 ACPH are analyzed in Figs.11, 12 and 13(a, b). For the heptane experiments of 30 cm, a large amount of energy in the form of radiation is released from the fuel gas undergoing oxidations. This allows an enhanced heat feedback to facilitate a faster thermal degradation of liquid with an accumulation of pyrolysis products inside the enclosure. Starting from about 200 s, the oxygen starvation begins and the oxygen-lean/fuel-rich hot upper layer is being formed with a rapid fall of oxygen concentration to about 5% (cf. Fig.13a). As shown in Fig.11(a, b), the ultra-fast growing fire becomes quickly oxygen limited with a concentration of about 10% nearby the fire source (Eq.12), resulting in a drastic decrease in combustion efficiency up to about 0.3. Variations in the theoretical HRR from 100 to 250 kW (cf. Fig.11) may be caused by the flame moving from the fuel pan towards oxygen available zone [7] in a vitiated air enclosure, named as phenomenon of ghosting flame. The impact of applying IVC procedure on the peak of about 250 kW in the theoretical HRR at 3 ACPH seems negligible. The heptane fire weakens earlier and finally stops with a reduction

in the fire duration by a factor of 40% by closing air intake (cf. Fig.11b). As illustrated in Fig.12(a, b), replacing heptane by dodecane leads to a sensitive change in HRR mainly due to a higher boiling point of dodecane (cf. Tab.1). The dodecane HRR reaches a plateau over a period of quasi steady state instead of a rapid heptane fire growth (cf. Fig.12). As compared to the heptane fire (cf. Fig.11), the dodecane fire generates a reduction in the theoretical HRR by a factor of 55% and the effective HRR by a factor of 40%. The dodecane fire exhaust takes place later by closing inlet vent (cf. Fig.12b) in comparison with the heptane fire (cf. Fig.11b). As a result, closing air intake extends the period of steady state burning by a factor of 40%, and air entrainment from the dilution duct and the leakage (Eq.4) allows to generate only a low HRR of about 50 kW. Starting from 1500 s, by closing air admission at 3 ACPH (cf. Fig.12b), the accumulated heat energy in smoke layer facilitate a faster thermal degradation of dodecane with a strong oscillation in the theoretical HRR. The fire extinction is followed by a rapid rise of oxygen concentration in smoke (cf. Fig.13) thanks to a return of air against the extracted smoke via the dilution duct. The calculated oxygen concentration is lower than the measured one with an error below 30% when the fire becomes under-ventilated. In relation to the experimental data, a deviation of the fire extinction delays in CFD simulation is more than 40%. This is mainly due to the shortcoming of a simple fire extinction model which is irrespective to various chemical reactions with complex kinetics depending on gas temperature. Moreover, in under-ventilated conditions, a deviation of the fire extinction delays exceeds ±100 s due to the worst repeatability during the various fire tests (cf. Fig.4b). It seems most likely that the discrepancies are due to a combination of the experimental uncertainties and the possible error in the numerical simulation.

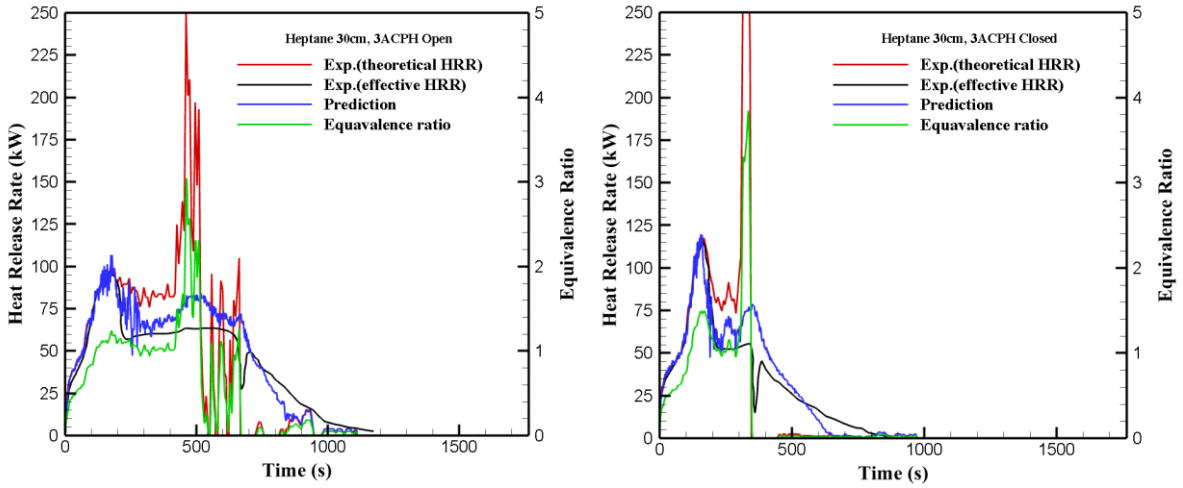

11a) Fire scenario 5 11b) Fire scenario 6

Figure 11. Impact of closing air intake on HRR for the under-ventilated heptane fires of 30 cm at 3 ACPH

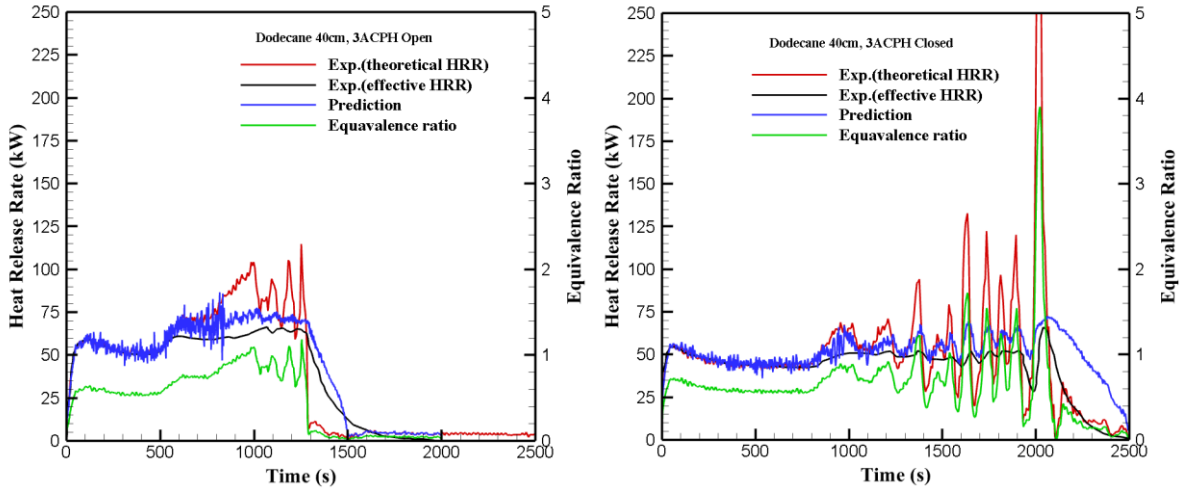

12a) Fire scenario 13 12b) Fire scenario 14

Figure 12. Impact of closing air intake on HRR for the under-ventilated dodecane fires of 40 cm at 3 ACPH

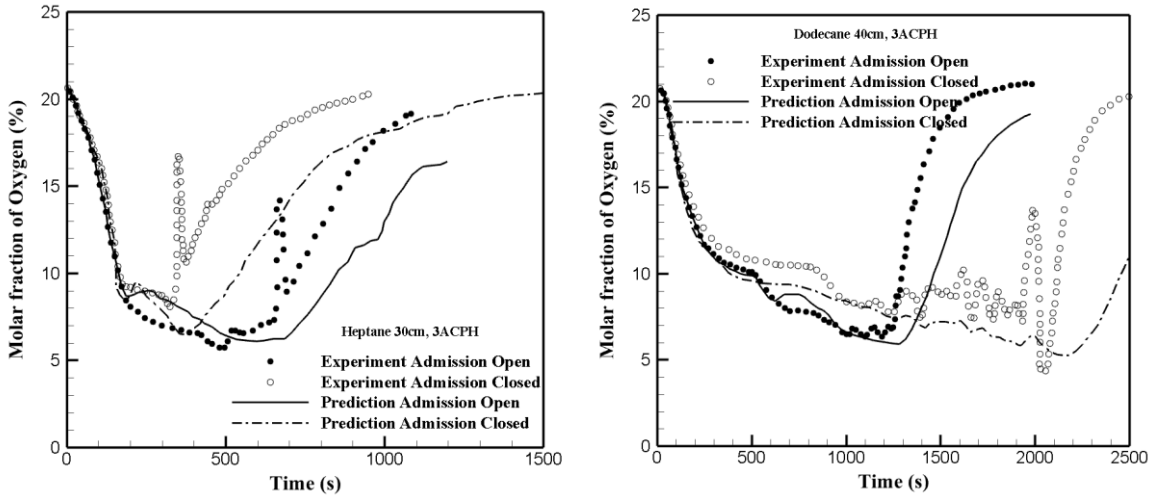

13a) Fire scenarios 5-6 13b) Fire scenarios 13-14

Figure 13. Histories of oxygen concentration at entrance of the extraction duct for the heptane pan of 30 cm and the dodecane pan of 40 cm at 3 ACPH

Effects of an increase of ACPH to 5 on the evolution of HRR for the heptane burning of 30 cm (scenarios 7-8) and the dodecane fire of 40 cm (scenarios 15-16) are shown in Figs.14 and 15(a, b). For the heptane fire, air intake at 5 ACPH (cf. Fig.14a) helps to reduce the maximal theoretical HRR by a factor of 30% as compared to that at 3 ACPH (cf. Fig.11a) due to a stronger fresh air entering the enclosure. By applying IVC procedure, variation of ACPH from 3 to 5 does not affect the peak of 250 kW in the theoretical HRR. Nevertheless, turning off air admission at 5 ACPH translates to a reduction in the maximal effective HRR from 150 kW (cf. Fig.14a) to 100 kW (cf. Fig.14b), that is to say by a factor of 30%. For the dodecane fire, air admission at 5 ACPH (cf. Fig.15a) generates a large amplitude in the theoretical HRR with a peak of 225 kW which is higher by a factor of 55% than that at 3 ACPH (cf. Fig.12a). Even with air intake at 5 ACPH, starting from 500 s, a fully developed fire becomes progressively ventilation-controlled with a drastic decrease in combustion efficiency to about 0.5. By closing

inlet vent at 5 ACPH, the maximal theoretical HRR and the effective HRR are reduced respectively to 90 and 60 kW (cf. Fig.15b) instead of 225 and 100 kW with air intake (cf. Fig.15a). However, by applying IVC procedure, duration of the steady state burning increases by a factor of 40% with a combustion efficiency of about 0.8. For the dodecane fire, air intake results in a drastic reduction in combustion efficiency from 0.75 (cf. Fig.12a) to 0.45 (cf. Fig.15a) with an increase of ACPH from 3 to 5. Inversely, closing air intake at 5 ACPH generates a high combustion efficiency of 0.75 (cf. Fig.15b) instead of 0.25 at 3 ACPH (cf. Fig.12b). In all the cases, combustion efficiency below 0.8 conducts to a non-negligible quantity of unburnt fuel [23]. The HRR reproduced by the oxygen limited combustion model (Eq.7) follows approximately the effective HRR (cf. Figs.14, 15).

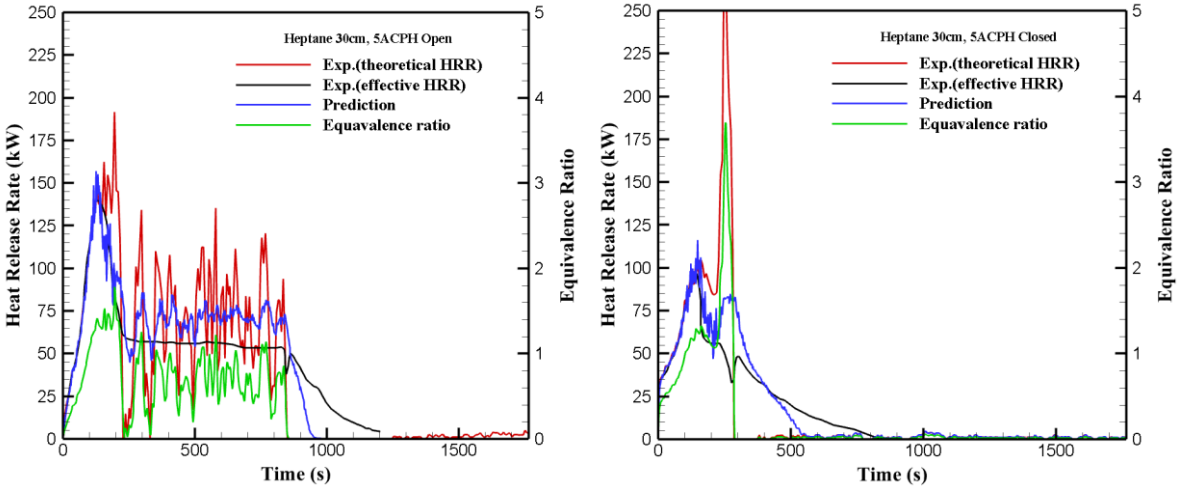

14a) Fire scenario 7 14b) Fire scenario 8

Figure 14. Impact of closing air admission on HRR for the under-ventilated heptane fires of 30 cm at 5 ACPH

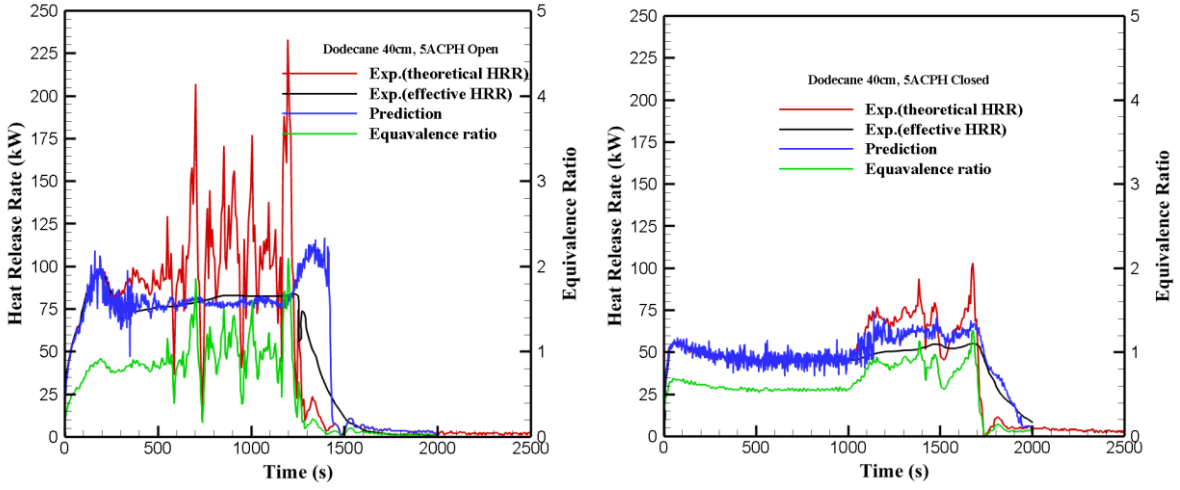

15a) Fire scenario 15 15b) Fire scenario 16

Figure 15. Impact of closing air intake on HRR for the under-ventilated dodecane fires of 40 cm at 5 ACPH

IV.4 Fire-induced pressure and inlet flow velocity

The coupling process between drop in pressure inside the enclosure and the inlet velocity is discussed for the heptane experiments of 30 cm at 3 and 5 ACPH (scenarios 5-8). The other fire scenarios present a similar trend with regarding the characteristic dependence between the compartment fire pressure and the air inlet velocity from the admission duct. Evolution of drop in pressure (P_0-P) versus time is illustrated in Fig.16(a-d). A typical behaviour is characterized by a peak of overpressure when the fire starts and a peak of drop in pressure when the fire extinction occurs. Closing air intake at 3 ACPH (cf. Fig.16a, b) does not affect a lot the peak of drop in pressure with about 160 Pa instead of 140 Pa with air intake. By applying IVC procedure, the strong oscillations of drop in pressure are preceded by a short spike up to zero due to the thermal confinement before extinction is achieved. The scenario of a fire in a confined and ventilated installation is a typical hazard during which a large variation in pressure is a key issue for the assessment of a dynamic confinement [26] in the nuclear safety area. The simulation and the measurement show that both fire growth rate and ACPH are found to be important for the expected peak of drop in pressure. As shown in Fig.16(c, d), there is a tendency to reduce the peak of drop in pressure from 160 to 120 Pa with an increase of ACPH from 3 to 5. This implies that air supply rate from the dilution duct and the leakage is expected to be less important at 5 ACPH, leading to a reduction in the maximal effective HRR (cf. Figs.14b, 15b) by applying IVC procedure.

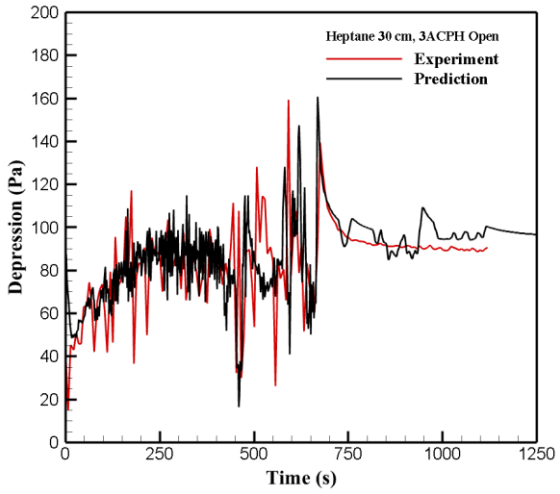

16a) Fire scenario 5

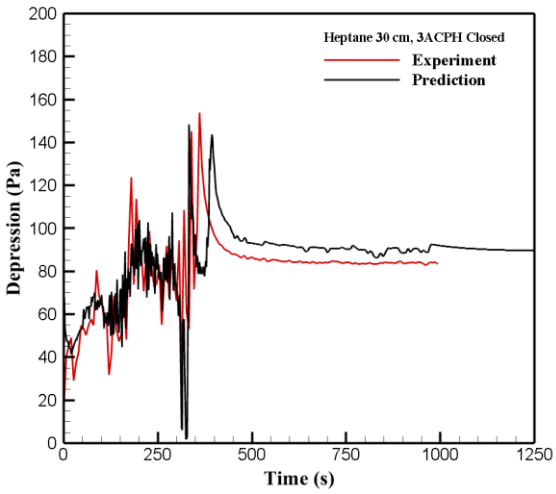

16b) Fire scenario 6

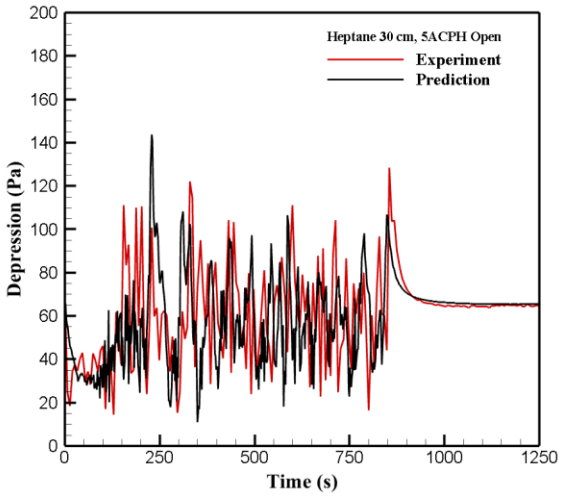

16c) Fire scenario 7

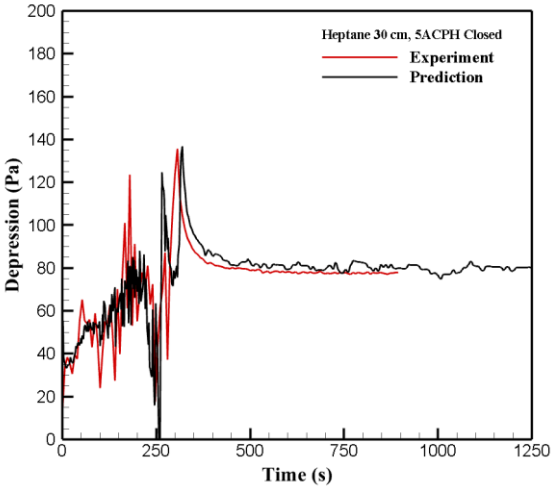

16d) Fire scenario 8

Figure 16. Evolution versus time of the measured and the calculated pressures for the heptane pan of 30 cm at 3 and 5 ACPH with a discrepancy within 15% in the peak

History of the inlet velocity at the admission duct for the same fire scenarios 5-8 is presented in Fig.17(a, b). In absence of the fire, the air inlet velocity varies from 0.1 to 0.55 m/s with an increase of ACPH from 3 to 5. Activating the fire induces a rapid increase in the inlet velocity of air entering the compartment as a result of a significant drop in pressure (cf. Fig.16). A high ACPH of 5 results in a faster inlet velocity of 3 m/s in peak instead of 1.5 m/s at 3 ACPH. Air entering the compartment with such a velocity enhances flow movements nearby the fire source and disturbs the flame structure, causing a strong oscillations of HRR (cf. Figs.14a, 15a). Oscillation of the inlet velocity follows closely fluctuation of the fire-induced pressure. Occurrence of flame extinction generates a constant supply of fresh air which favours an increase in oxygen concentration inside the enclosure (cf. Figs.10, 13).

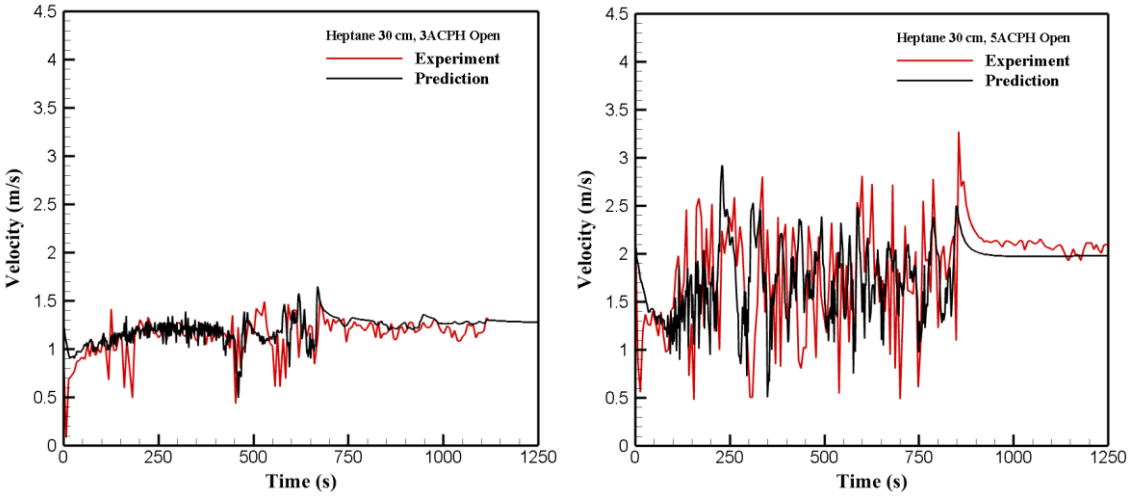

17a) Fire scenario 5 17b) Fire scenario 7

Figure 17. Evolution of the measured and the calculated inlet velocities at the admission duct for the heptane pan of 30 cm at 3 and 5 ACPH

Regardless of the fire scenarios, the overall oscillations of drop in pressure and inlet velocity are reproduced well by the HVAC module which requires knowledge of the gas temperature development and the leakage flows [11]. The characteristic dependence between air inlet and pressure is quantitatively captured by the models.

IV.5 Ignition risk of unburnt pyrolyzates

In under-ventilated conditions, the excess combustible gas from pyrolysis of liquid fuel contribute to an accumulation of unburnt gases such as carbon monoxide, hydrogen and all unburnt hydrocarbons at entrance of the extraction duct. Based on the Burgess-Wheeler's law [27], Lower Flammability Limit (LFL) and Upper Flammability Limit (UFL) of each fuel and gas mixtures as a function of fuel molar fraction X_i as well as gas temperature are expressed as follows :

$$LFL_i(T) = LFL_i(T_0)\left[1 - \frac{T - T_0}{1300 - T_0}\right] \quad \text{and} \quad LFL(T) = 100 \times \left[\sum_i \frac{X_i}{LFL_i(T)}\right]^{-1} \qquad (15)$$

$$UFL_i(T) = UFL_i(T_0)\left[1+\frac{T-T_0}{1412-T_0}\right] \quad \text{and} \quad UFL(T) = 100\times\left[\sum_i \frac{X_i}{UFL_i(T)}\right]^{-1} \qquad (16)$$

According to the Babrauskas's extinction/ignition criteria [28], the risk of auto-ignition occurs when the range of unburnt fuel concentration is between LFL and UFL at the point of Auto-Ignition Temperature (AIT). The values of LFL_i and UFL_i at T_0=25°C as well as AIT for the four fuel species are summarized in Table 3 [28]. In the current enclosure fire, the concentration of the unburnt volatiles is largely below UFL with a value of about 20%. The Zabetakis's work [29] shows that for the majority of hydrocarbons, LFL decreases of approximately 8% for an increase of the gas temperature of 100°C. The self-ignition point represents the minimum temperature at which a flammable mixture ignites spontaneously in absence of an ignition source such as a spark or a flame. Determination of the self-ignition temperature is difficult because it depends on the experimental conditions and complex kinetics reactions attached to the fuel type (cf. Tab.3). Usually, whatever the family of hydrocarbons considered, AIT decreases with the length of the carbon chain and becomes almost constant for long chains [28].

Table 3. Values of the AIT and LFL/UFL at T_0=25°C for the four fuel species

Parameter	CO	H_2	Dodecane	Heptane
LFL (T_0=25°C)	12.5%	4%	0.6%	1.05%
UFL (T_0=25°C)	74%	75%	4.7%	6.7%
AIT (°C)	588	520	204	223

It is necessary to check if the composition of chemical species can be numerically reproduced for assessing an ignition risk of unburnt pyrolyzates. The calculated and the measured concentrations of carbon monoxide, hydrogen and unburnt hydrocarbons for the heptane experiments of 30 cm (scenarios 5-6) and the dodecane experiments of 40 cm (scenarios 13-14) at 3 ACPH are compared in Figs.18 and 19(a-c). During the initial period before 350 s, the fire is in over-ventilated conditions with a negligible production of unburnt species. The under-ventilated regime with a production of unburnt gases is reached between 250 and 750 s for the heptane fire, and between 500 and 1500 s for the dodecane fire. For the heptane fire (cf. Fig.18), production of CO is greater than the two other unburnt gases, and the impact of applying IVC procedure on the peak of unburnt species concentration seems negligible. Dodecane with a longer carbon chain produces more unburnt gases such as CO and C_xH_y than heptane. As shown in Fig.19, the growth rate of the unburnt gases from the dodecane fire becomes faster with the air inlet open, and applying IVC procedure generates a reduction in unburnt species concentration. A deviation of the calculated peak in unburnt fuels concentration in relation to the experimental data is more than five times. This is mainly attributed to the shortcoming of an infinitely fast EDC combustion model [11]. Besides, air feeding towards the enclosure due to drop in pressure has an influence on the distribution of unburnt pyrolyzates. In comparison with the experimental data, the calculated species concentration seems qualitatively promising for the heptane fire. The attempt to numerically reproduce the minor species concentration for the dodecane fire was not successful.

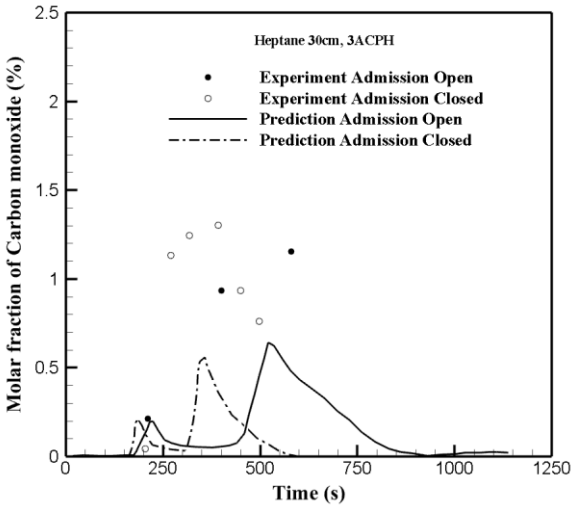

18a) Carbon monoxide

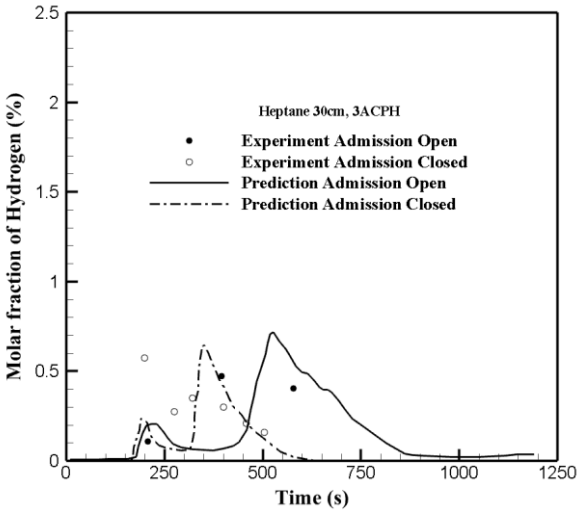

18b) Hydrogen

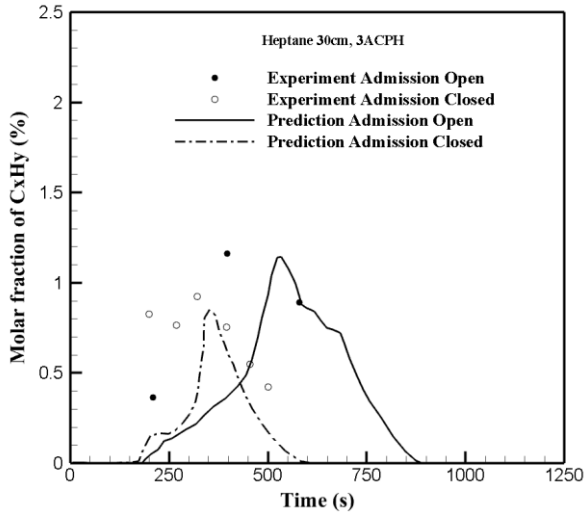

18c) Hydrocarbon

Figure 18. Histories of the unburnt species concentration at entrance of the extraction duct for the heptane pan of 30 cm at 3 ACPH (scenarios 5-6)

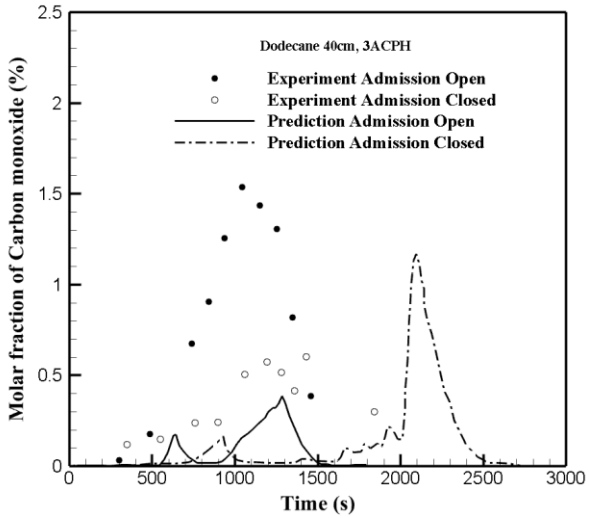

19a) Carbon monoxide

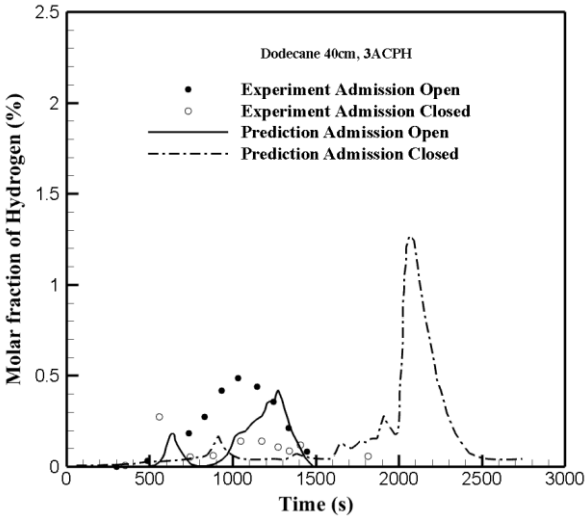

19b) Hydrogen

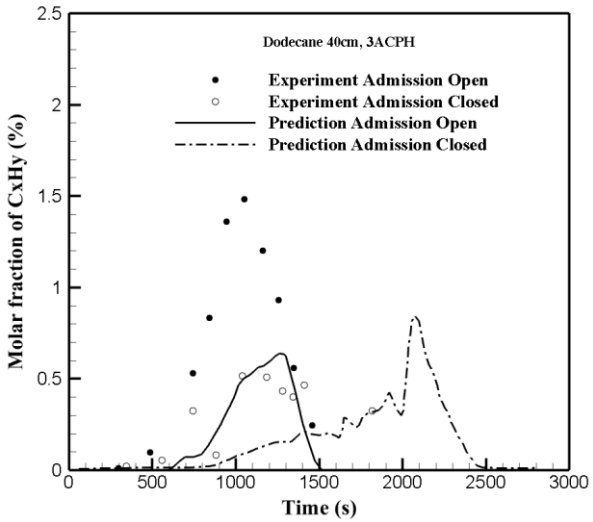

19c) Hydrocarbon

Figure 19. Histories of the unburnt species concentration at entrance of the extraction duct for the dodecane pan of 40 cm at 3 ACPH (scenarios 13-14)

The cumulative concentrations of the unburnt species as C_xH_y, CO, H_2 in addition to the corresponding LFL near the extraction duct for the heptane pan of 30 cm and the dodecane pan of 40 cm at 3 and 5 ACPH are presented in Figs.20 and 21(a-d). For the heptane fire at 3 ACPH (cf. Fig.20a, b), a delay of about 400 s with the air inlet open and of 200 s by applying IVC procedure is needed for reaching the threshold value of LFL. This implies that the delay time for an eventual ignition of unburnt pyrolyzates is reduced by a factor of 40% by applying IVC procedure at 3 ACPH. A high ACPH of 5 (cf. Fig.20c, d) reduces an ignition risk near the extraction duct since concentration of unburnt pyrolyzates is below LFL due to more air feedings towards the enclosure. For the dodecane fire, a low ACPH of 3 (cf. Fig.21a, b) induces a potential ignition risk of unburnt pyrolyzates starting from 700 s with the air inlet open and 1100 s by applying IVC procedure. This means that at 3 ACPH, the dodecane fire contributes to a prolongation in the delay time of ignition risk by a factor of about 1.5 times with the air inlet open and of about 3 times by applying IVC procedure. At 5 ACPH (cf. Fig.21c, d), concentration of unburnt pyrolyzates reaches LFL at around 500 s with the air inlet open, and however, stays below LFL till 1300 s by applying IVC procedure.

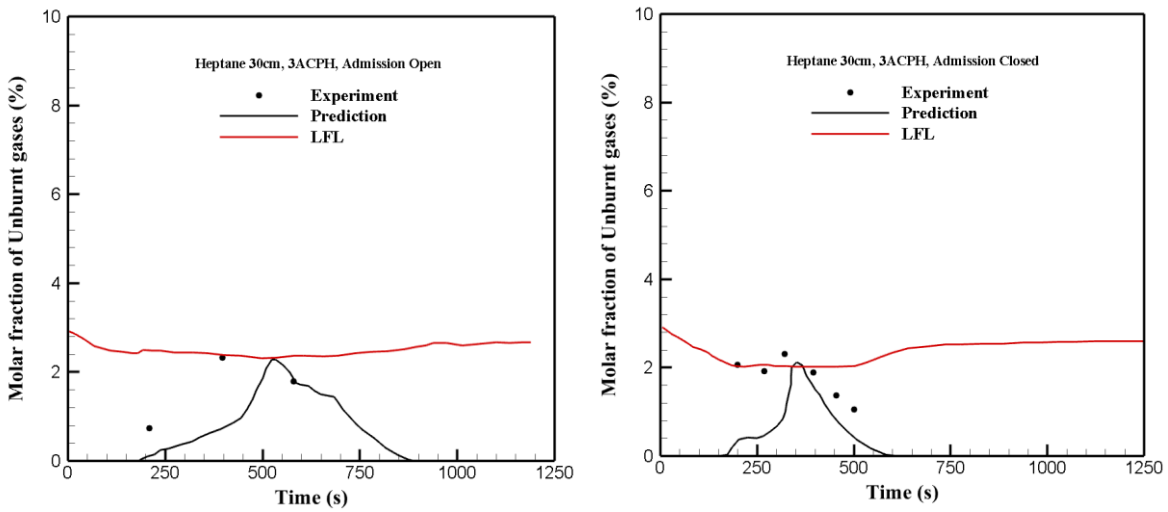

20a) Fire scenario 5

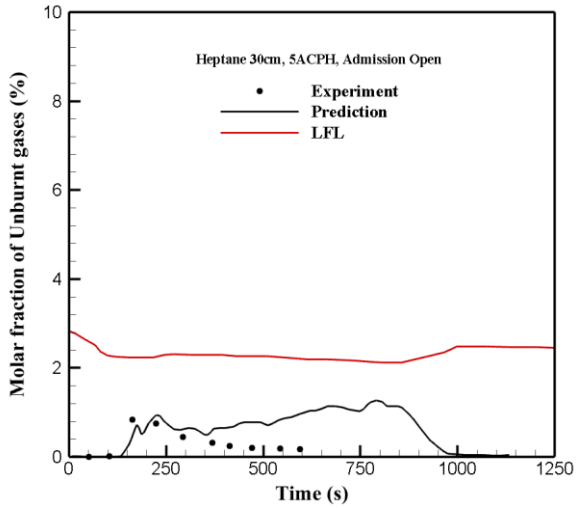

20b) Fire scenario 6

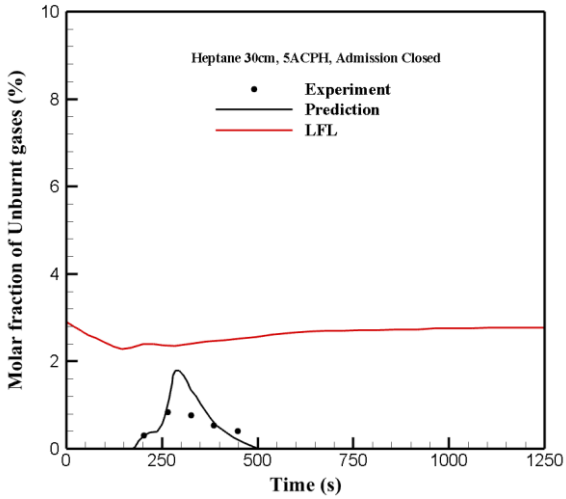

20c) Fire scenario 7

20d) Fire scenario 8

Figure 20. Impact of closing air intake on concentration of the unburnt species at entrance of the extraction duct for the heptane pan of 30 cm at 3 and 5 ACPH

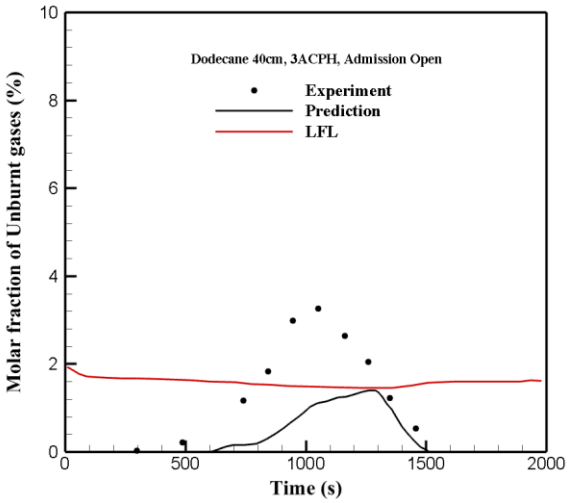

21a) Fire scenario 13

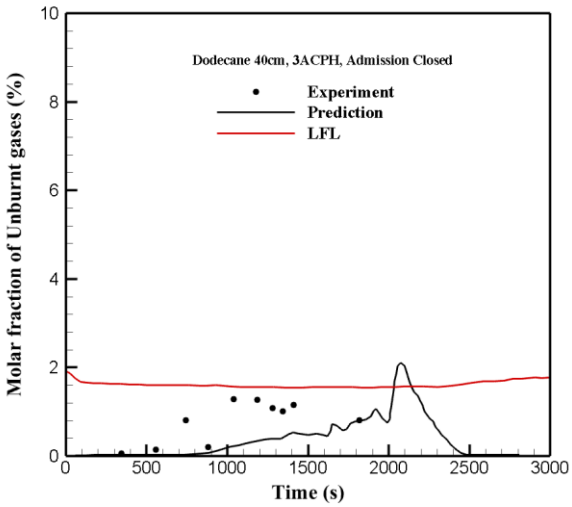

21b) Fire scenario 14

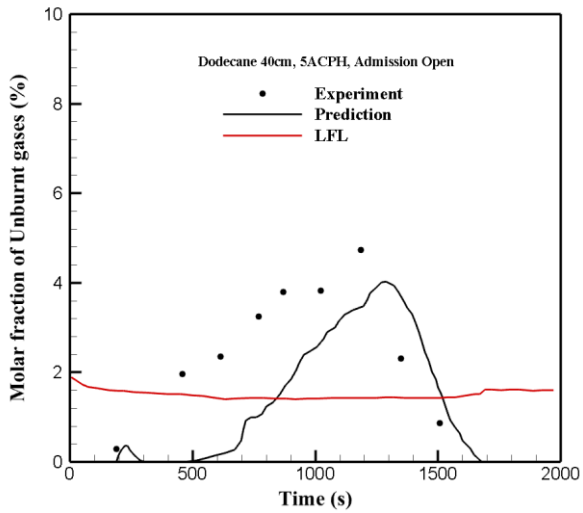

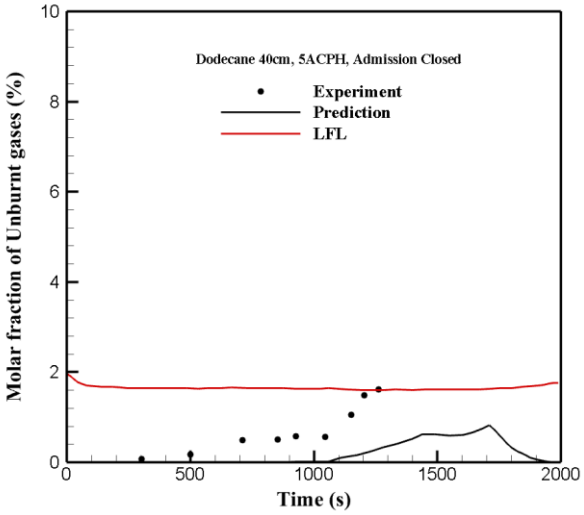

21c) Fire scenario 15 21d) Fire scenario 16

Figure 21. Impact of closing air intake on concentration of the unburnt species at entrance of the extraction duct for the dodecane pan of 40 cm at 3 and 5 ACPH

Note that the self-ignition laws (Eqs.15, 16) [27, 28] are established for homogeneous and static medium. In the current study, the environment is dynamic and heterogeneous with sudden variations in temperature and composition of the fuel-air mixture. Therefore, several approximations are made for assessing the ignition risk which relies on only the heptane or the dodecane AIT (cf. Tab.3). Figs.22 and 23(a, b) show the histories of the gas temperature at entrance of the extraction duct at 3 and 5 ACPH for the heptane pan of 30 cm and the dodecane pan of 40 cm.

For the heptane fire of 30 cm (cf. Fig.22a, b), with the air inlet open, the gas temperature increases sharply to reach a peak value of about 280°C at 3 ACPH and 340°C at 5 ACPH during the early stage. Then, the air inlet open generates a decrease of the temperature to a plateau in a quasi-steady period with a value of 260°C when the fire becomes under-ventilated. By applying IVC procedure, the fire exhaust occurs early with a sharp drop in the gas temperature. Applying IVC procedure at 3 ACPH induces an increase of gas temperature (cf. Fig.22a), and inversely, this operation at 5 ACPH reduces the peak of gas temperature from 340°C to 300°C (cf. Fig.22b). As illustrated in Fig.13a for a low ACPH of 3, there is a sudden rise of oxygen up to a value above 15% near the extraction duct with a delay of about 700 s with the air inlet open and of 350 s by applying IVC procedure. This is attributed to a return of air against the extracted smoke caused by a strong drop in pressure (cf. Fig.16) at the fire extinction point. This is ideal for triggering auto-ignition of unburnt pyrolyzates near the extraction duct, and such an ignition phenomenon was visually identified. At 5 ACPH, there is no ignition risk of unburnt pyrolyzates near the extraction duct since concentration of unburnt pyrolyzates (cf. Fig.20c, d) is below LFL although the gas temperature is above the heptane AIT (cf. Tab.3).

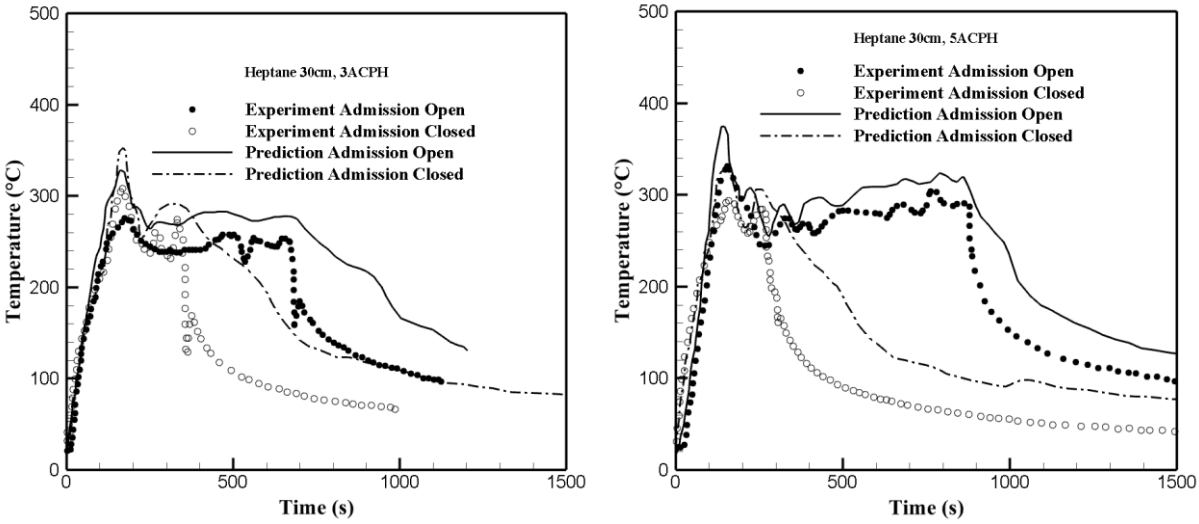

22a) Fire scenarios 5-6 22b) Fire scenarios 7-8

Figure 22. Impact of closing air intake on the gas temperature at entrance of the extraction duct for the heptane pan of 30 cm

For the dodecane pan of 40 cm at 3 ACPH (cf. Fig.19a), the gas temperature near the extraction duct increases monotonously during a long time of about 1200 s with the air inlet open and of

1800 s by applying IVC procedure. During this period, the energy released during combustion allows the gas temperature to raise above the dodecane AIT (cf. Tab.3). Thanks to a sudden increase of oxygen concentration up to a value of about 15% (cf. Fig.13b), all necessary conditions are reached to trigger an auto-ignition of unburnt pyrolyzates, characterized by a typical flame temperature of about 500°C. By applying IVC procedure, occurrence of auto ignition near the extraction duct was observed after a long-time delay of about 2000 s at 3 ACPH and 1600 s at 5 ACPH. Applying IVC procedure generates an increase in the time delay for reaching an auto-ignition by a factor of 40% at 3 ACPH and by 20% at 5 ACPH. An auto-ignition of unburnt pyrolyzates is visually identified for the tested fire scenarios 13-16. However, with the air inlet open at 3 ACPH and by applying IVC procedure at 5 ACPH, the flame temperature at ignition point was not experimentally detected by the thermocouple although concentration of unburnt pyrolyzates is above LFL and the gas temperature is above the dodecane AIT. The general instantaneous flow circulation at the fire extinction point inside the compartment is qualitatively illustrated in Fig.24. Near entrance of the extraction duct, a return of fresh air against the extracted smoke caused by a drop in pressure during the fire extinction generates a strong flow perturbation. In such a heterogeneous medium (cf. Fig.24), identification of a random phenomenon in space and time as auto-ignition by using thermocouples is not always successful. The numerical results from FDS6.5 seem not credible as a support to visualize an auto-ignition of unburnt pyrolyzates due to lack of the chemical processes with the elementary reactions and species [30].

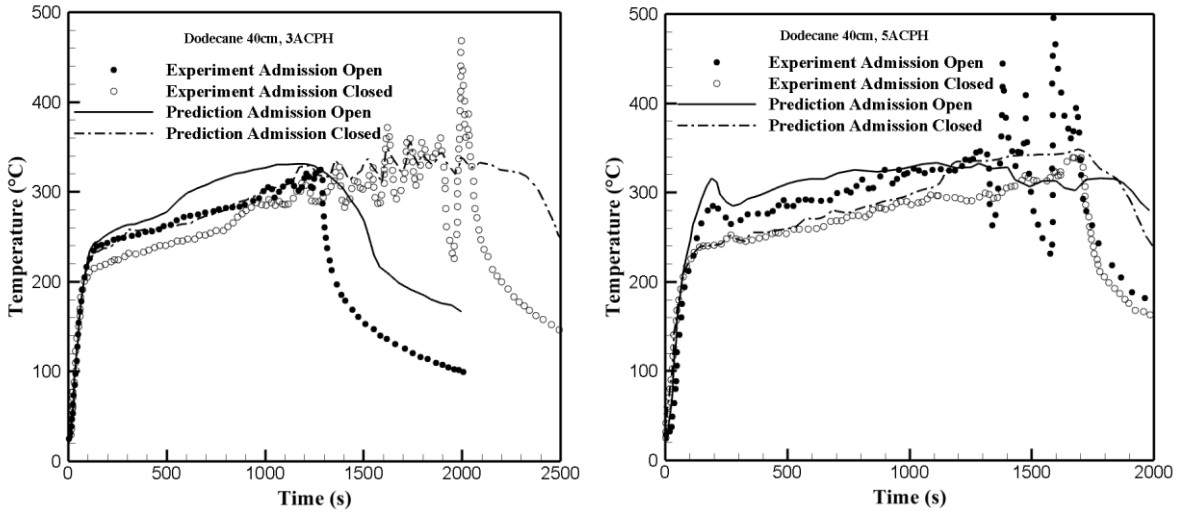

23a) Fire scenarios 13-14 23b) Fire scenarios 15-16

Figure 23. Impact of closing air intake on the gas temperature at entrance of the extraction duct for the dodecane pan of 40 cm

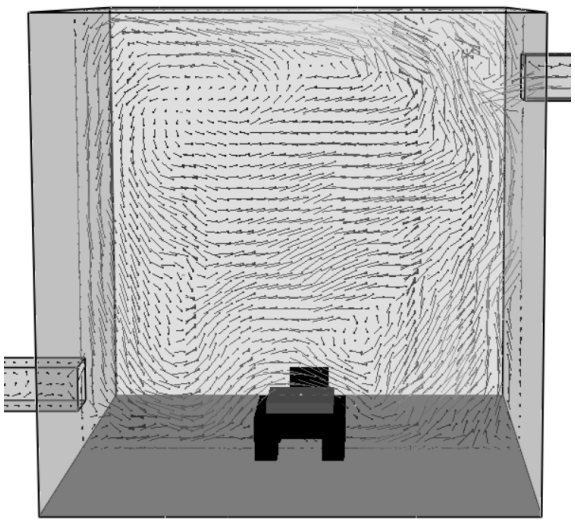

Figure 24. Illustration of the instantaneous flow circulation inside the compartment at the fire extinction point for 3 ACPH with the air inlet open (scenario 13)

The dodecane experiments of 30 cm (scenarios 9-12) and the heptane experiments of 23 cm (scenarios 1-4) correspond to well ventilated fires. Amount of unburnt pyrolyzates accumulated near the extraction duct is negligible, and thus there is no ignition risk. As shown in Fig.25(a, b), by applying IVC procedure to the dodecane fire, the gas temperature decreases rapidly to a value below the dodecane AIT, leading to an insufficient heat feedback for thermal degradation of dodecane. By applying IVC procedure to the heptane pan of 23 cm (cf. Fig.26a, b), a plateau with a temperature of about 200°C is maintained in a longer duration, following the trend of HRR (cf. Fig.9).

Overall, in under-ventilated conditions (cf. Figs.22, 23), the temperature peak is over-predicted by 20% for the heptane fire, and by 40% for the dodecane fire. A good agreement between the calculated and the measured gas temperature is found for a well-ventilated fire (cf. Figs.25, 26) with an over-prediction below 20% for the dodecane fire.

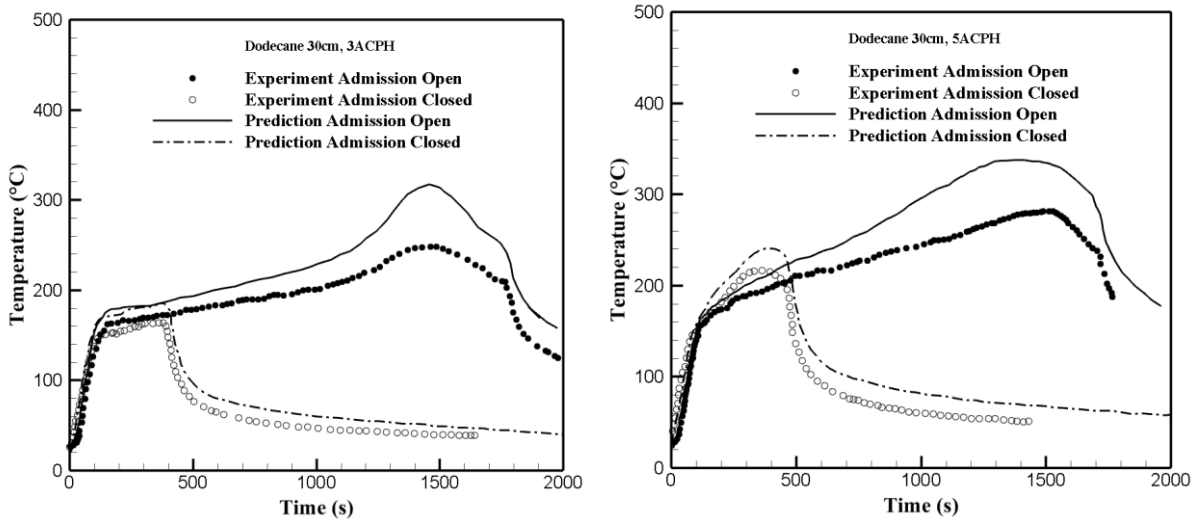

25a) Fire scenarios 9-10 25b) Fire scenarios 11-12

Figure 25. Impact of closing air intake on the gas temperature at entrance of the extraction duct for the dodecane pan of 30 cm

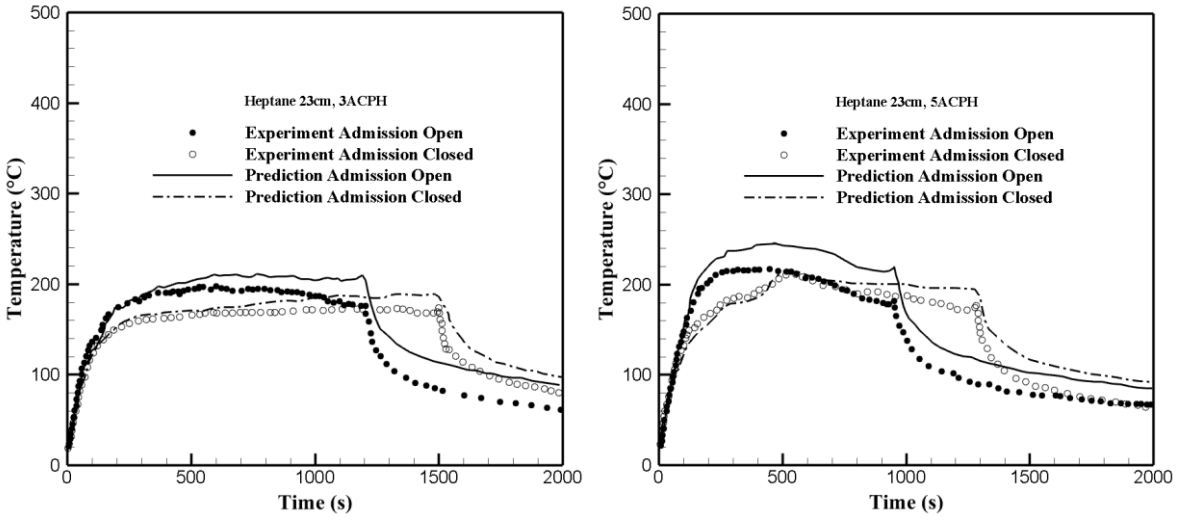

26a) Fire scenarios 1-2 26b) Fire scenarios 3-4

Figure 26. Impact of closing air intake on the gas temperature at entrance of the extraction duct for the heptane pan of 23 cm

V. CONCLUSIONS

The different fire scenarios were simulated experimentally and numerically by combining the four variables such as pan size, ACPH, air intake and fuel type (heptane and dodecane) in addition to an IVC procedure, i.e., limit the supply of fresh air into the compartment, thus restricting the available oxygen to that already in the compartment. The purpose of the overall research consists in identifying the consequences of applying IVC procedure on the compartment fires development in various fire dynamic regimes, and auto-ignition of unburnt pyrolyzates that have accumulated in sufficient concentration in the upper smoke layer due to limited oxygen.

These findings indicate that when the admission duct is closed, duration of a well-ventilated heptane fire becomes longer, but with a reduction in HRR. Inversely, for a well-ventilated dodecane fire, applying IVC procedure translates to a significant reduction in duration of fire due to insufficient heat feedback for its thermal degradation. As long as the heptane fire is ventilation controlled, applying IVC procedure translates to the most severe conditions for an eventual auto-ignition of unburnt pyrolyzates due to a significant thermal degradation of liquid fuel. In under-ventilated conditions, a heptane fire extinction happens early in comparison with a dodecane fire, as long as the admission duct is closed. By applying IVC procedure, an under-ventilated dodecane fire can be established for sufficiently long (in this case, more than 33 min) with a sensitive reduction in HRR. It is found that applying IVC procedure to the dodecane fire reduces the possibility of a rapid growth rate, and as a result, contributes to a prolongation in ignition delay time of unburnt pyrolyzates. For the fire scenarios with GER above 1.5, a gas temperature above AIT is usually maintained for sufficiently long time, and amount of accumulated unburnt pyrolyzates is above LFL. There is a significant risk of auto-ignition of unburnt pyrolyzates at entrance of the extraction duct when a return of air from the dilution duct occurs due to a sudden drop in pressure at the fire extinction point.

In the simulations of these experiments, HRR, oxygen concentration, pressure and gas temperature are calculated accurately as long as the fire is over-ventilated with GER below 0.7. On the basis of global extinction/ignition criteria, the numerical tool (FDS6.5) is useful through the post-processing for assessing auto-ignition of unburnt pyrolyzates as well as dynamic

confinement by prescribing a series of compartment fire scenarios. However, the code FDS6.5 is not credible to reproduce the phenomena of periodic oscillations with flame presence/absence nearby the fire source in under-ventilated conditions, as well as a random phenomenon as auto-ignition of unburnt pyrolyzates. A detailed chemical reactions with complex kinetics depending on gas temperature in addition to an extremely small grid size may be capable of fully resolving the characteristic flame oscillations, making practical fire simulations difficult. Predictive simulations of liquid pool fires have to properly take into account the liquid-phase by, e.g., lateral convection induced by the temperature gradients at liquid surface via heat feedback from the hotter combustion products. An experimental database on heat flux, owing to pyrolysis of an inflammable liquid, is needed for validation of the numerical tool. The future investigation aims also to improve the evaluation of auto-ignition of unburnt pyrolyzates by using a CCD camera instead of thermocouples.

REFERENCES

[1] L. Audouin, L. Rigollet, H. Prétrel, W. Le Saux, M. Rowekamp, OECD Prisme project : Fires in confined and ventilated nuclear-type multi-compartments –Overview and main experimental results, Fire Safety Journal, 62B (2013), 80-101.

[2] H.Prétrel, P. Querre, M. Foreestier, Experimental study of burning rate behavior in confined and ventilated fire compartments, Fire Safety Science, 8 (2005), 1217-1228.

[3] S. Vilfayeau, N. Ren, Y. Wang, A. Trouvé, Numerical simulation of under-ventilated liquid-fueled compartment fires with flame extinction and thermally-driven fuel evaporation. Proceedings of the Combustion Institute 35 (2015), 2563–2571.

[4] B.Y. Lattimer, D.T. Ewens, U. Vansburger, R.J. Roby, Transport and oxidation of compartment fire exhaust gases in an adjacent corridor, Journal of Fire Protection Engineering 6 (1994), 163-181.

[5] A. S. X. Loo, A. Coppalle, J. Yon, P. Aîné, Time-dependent smoke yield and mass loss of pool fires in a reduced-scale mechanically ventilated compartment, Fire Safety Journal, 81 (2016), 32-43.

[6] C.L. Beyler, Major species production by diffusion flames in a two-layer compartment fire environment, Fire Safety Journal, 10 (1986), 47-56.

[7] Takeda N, Oscillatory phenomenon and inverse temperature profile appearing in compartment fires, Combustion and Flame, 61 (1985), 103-105.

[8] J. Lassus, E. Studer, J.P. Garo, J.P. Vantelon, P. Jourda, P. Aine, Influence of ventilation on ignition risk of unburnt gases in the extraction duct of under ventilated compartment fire. Combustion Science and Technology, 182 (2010), 517-528.

[9] H.Prétrel, J.M. Such, Effect of ventilation procedures on the behavior of a fire compartment scenarios, Nuclear Engineering and Design 235 (2005), 2155–2169.

[10] Simo Hostikka, Rahul Kallada, Umar Riaz, Topi Sikanen, Fire-induced pressure and smoke spreading in mechanically ventilated buildings with air-tight envelopes, Fire Safety Journal, 91 (2017), 380-388.

[11] K. Mcgrattan, R. Mcdermott, S. Hostikka and J. Floyd, Fire Dynamics Simulator (Version 6), User's guide, NIST Special Publication (2018).

[12] E.E. Zukoski, Fluid dynamics aspects of room fires, First International Symposium on Fire Safety Science, (1984), 1-30.

[13] B. Manescau, L. Courty, L. Acherar, B. Coudour, H. Y. Wang, J.P. Garo, Ventilation conditions effects during a fire in a reduced scale room, Process Safety and Environmental Protection, 144 (2020), 263-272.

[14] S. Brohez, C. Delvosalle, G. Marlair, A two-thermocouple probe for radiation corrections of measured temperatures in compartment fires, Fire Safety Journal, 39:5 (2004), 399-411.
[15] A. Murty Kanury, Introduction to Combustion Phenomena, New York: Gordon, (1984) ISBN 0-677-02690-0.
[16] D. Stroup and A. Lindeman, Verification and validation of selected fire models for nuclear power plant applications. NUREG-1824, supplement 1, United States Nuclear Regulatory Commission, Washington, DC, (2013), 37-48.

[17] T. Sikanen and S. Hostikka, Predicting the heat release rates of liquid pool fires in mechanically ventilated compartments, Fire Safety Journal, 91(2017), 266-275.
[18] L. Acherar, H. Y. Wang, J.P. Garo and B. Coudour, Impact of air intake position on fire dynamics in mechanically ventilated compartment, Fire Safety Journal, 118 (2020), 103210.
[19] Ross, H. D. and Miller F. J. Flame spread across liquid pools with very low speed opposed or concurrent air flow, Twenty-Sixth Symposium (International) on Combustion, The Combustion Institute, Pittsburgh, , 27:2 (1998), 2723-2729.
[20] V. Babrauskas, Estimating large pool fire burning rates, Fire Technology 19, 1983, 251-261.

[21] B. Manescau, H.Y. Wang, B. Coudour and J.P. Garo, Influence of heat tightness of an enclosure fire on ignition risk of unburnt gases in a connected exhaust system – An experimental study, Fire Safety Journal, 109 (2019), 102867.

[22] N.P. Bryner, E.L. Johnsson, W.M. Pitts, Carbon monoxide production in compartment fires: reduced-scale enclosure test facility, National Institute of Standards and Technology, (1994), NISTIR-5568.

[23] SFPE Handbook of fire protection engineering, National Fire Protection Association, Mohammed M. Khan, Archibald Tewarson and Marcos Chaos, Chapter 36, Combustion Characteristics of Materials and Generation of Fire Products , Fifth Edition (2016), 1143-1232.

[24] Moss, J.B., Stewart, C.D., Young, K.J., Modelling soot formation and burnout in a high temperature laminar diffusion flame burning under oxygen-enriched conditions, Combustion and Flame, 101 (1995), 491-500.
[25] Marc L. Janssens, Measuring rate of heat release by oxygen consumption, Fire Technology (1991), 234-249.
[26] Pretrel H., Le Saux W, Audouin L., Pressure variations induced by a pool fire in a well confined and force-ventilated compartment, Fire Safety Journal, 52 (2012), 11-24.

[27] M. J. Burgess and R. V. Wheeler. The lower limit of inflammation of mixtures of parrafin hydrocarbons with air, Journal of Chemical Society Transactions, XCIX (1911), 2013-2030.
[28] Ignition Handbook, Fire Science Publishers, Babrauskas, V., Chapter 4, (2003), 41-140.

[29] M. G. Zabetakis. Flammability characteristics of combustible gases and vapours, US Dept of the Interior, Bureau of Mines, (1965), bulletin 627.
[30] Melguizo Gavilanes and Shepherd, J.E. Hot surface ignition and flow separation, 25th ICDERS, Aug. 2-7, 2015, Leeds, UK.